BAJECE

e-mail: editor@bajece.com

Balkan Journal of Electrical & Computer Engineering

An International Peer Reviewed, Referred, Indexed and Open Access Journal

www.bajece.com

Vol : 5
No : 1
Year : 2017
ISSN : 2147 - 284X

This journal is supported by the Istanbul Technical University.
It is abstracted and indexed in, Index Google Scholarship, the PSCR, Cross ref, DOAJ, Research Bible, Indian Open Access Journals (OAJ), Institutional Repositories (IR), J-Gate (Informatics India), Ulrich's, ResearchGate, International Society of Universal Research in Sciences, DRJI, EyeSource, Cosmos Impact Factor, Cite Factor, SIS Scientific Indexing Service, IIJIF, iiiFactor.

Aim & Scope
The journal publishes original papers in the extensive field of Electrical-Electronics and Computer engineering. It accepts contributions which are fundamental for the development of electrical engineering, computer engineering and its applications, including overlaps to physics. Manuscripts on both theoretical and experimental work are welcome. Review articles and letters to the editors are also included.
Application areas include (but are not limited to): Electrical & Electronics Engineering, Computer Engineering, Software Engineering, Biomedical Engineering, Electrical Power Engineering, Control Engineering, Signal and Image Processing, Communications & Networking, Sensors, Actuators, Remote Sensing, Consumer Electronics, Fiber-Optics, Radar and Sonar Systems, Artificial Intelligence and its applications, Expert Systems, Medical Imaging, Biomedical Analysis and its applications, Computer Vision, Pattern Recognition, Robotics, Industrial Automation.

BAJECE
Balkan Journal of Electrical & Computer Engineering
An International Peer Reviewed, Indexed and Open Access Journal

ISSN: 2147- 284X
Vol: 5
No : 1
Year: February 2017

CONTENTS

BALKAN JOURNAL OF ELECTRICAL & COMPUTER ENGINEERING
(An International Peer Reviewed, Indexed and Open Access Journal**)**

Contact
Istanbul Technical University
Department of Electrical Engineering
Ayazaga Campus, Maslak, Istanbul-Turkey

Web: https://www.bajece.com
http://dergipark.gov.tr/bajece/
e-mail: editor@bajece.com

Production of Circular Stator Current Trajectory in Multi-Phase Induction Drive Under Open Phase Fault Condition

A. Pitrėnas, D. Uznys, and D. Beištaras

***Abstract*—In this paper multi-phase induction drive with a frequency converter is researched under open phase fault condition. Control strategy of stator voltage phase shift is proposed for dealing with over-currents during steady state. Symmetry of stator current trajectory is achieved. Experiments with six-phase induction motor without a neutral wire under one open phase condition were carried out.**

Index Terms—**Current trajectory, induction motor, frequency inverter, multi-phase drive, open phase fault, scalar control.**

I. Introduction

MULTI-PHASE induction motors have numerous advantages compared to three-phase induction motors such as reduced torque pulsations, magnetic flux harmonic reduction, reduction on the rotor harmonic current losses, dc link current harmonics and higher reliability under the loss of one or more stator phases [1-4].

Multi-phase induction motors are used in wind power systems, electrical and hybrid vehicles [5], electric ship propulsion [6], in 'more electric aircraft' actuators and in safety-critical applications, such as aerospace or military naval drives, where fault tolerance is a desirable feature [7].

Induction motor failures can be divided into the following categories: bearing faults, stator and rotor faults, eccentricity and vibration faults. The most common failures occur in the stator and rotor.

Stator faults are open circuit or short-circuit of one or more stator windings, coil-to-coil, phase to phase and coil to ground. These kinds of faults can be caused by local damage to insulation, extreme electrical operating conditions or extreme ambient conditions, leading to different phase winding short circuit, which may result in further open phase faults of one or more phase windings [8, 9].

A. PITRĖNAS, is with Department of Automation, Vilnius Gediminas Technical University and Vilnius College of Technologies and Design, Vilnius, Lithuania, (e-mail: aurelijus.pitrenas@vgtu.lt).

D. UZNYS, is with Department of Automation, Vilnius Gediminas Technical University, Vilnius, Lithuania, (e-mail: donatas.uznys@vgtu.lt).

D. BEIŠTARAS is with Department of Automation, Vilnius Gediminas Technical University and Vilnius College of Technologies and Design, Vilnius, Lithuania, (e-mail: dominykas.beistaras@vgtu.lt).

Manuscript received August 15, 2016; accepted October 21, 2016.
DOI: 10.17694/bajece.292281

Open phase fault is the most common fault that increases peak values of currents in the rest of the phases significantly. Under these conditions trajectory of rotating magnetic field becomes elliptical.

It is important to find appropriate methods to obtain circular currents trajectories in six-phase motors for single-phase fault. Therefore, a control strategy of stator voltage phase shift is proposed for dealing with over-currents during steady state.

II. Stator Open-Phase Fault

Induction motor torque depends on the generated stator magnetic flux. Ideally, the magnetic flux trajectory is circular.

A six-phase squirrel-cage induction motor with isolated neutral point is investigated. Measuring the magnetic flux directly is complicated, therefore stator phase currents are measured and the trajectory of magnetic flux is calculated instead. Current trajectory in stationary frame is calculated by the following expressions:

$$i_{sd} = 0 \cdot i_{sA} + \left(\sin\left(\frac{\pi}{3}\right)\cdot i_{sB}\right) + \left(\sin\left(\frac{2\pi}{3}\right)\cdot i_{sC}\right) + \left(\sin(\pi)\cdot i_{sD}\right) + \left(\sin\left(\frac{4\pi}{3}\right)\cdot i_{sE}\right) + \left(\sin\left(\frac{5\pi}{3}\right)\cdot i_{sF}\right) \quad (1)$$

$$i_{sq} = i_{sA} + \left(\cos\left(\frac{\pi}{3}\right)\cdot i_{sB}\right) + \left(\cos\left(\frac{2\pi}{3}\right)\cdot i_{sC}\right) + \left(\cos(\pi)\cdot i_{sD}\right) + \left(\cos\left(\frac{4\pi}{3}\right)\cdot i_{sE}\right) + \left(\cos\left(\frac{5\pi}{3}\right)\cdot i_{sF}\right) \quad (2)$$

Where: i_{sd} – is d component of stator current of stationary frame; i_{sq} – is q component of stator current of stationary frame; i_{sA} … i_{sF} – are instantaneous stator phase currents.

Stator current trajectory in healthy mode is circular as all instantaneous currents have the same peak values and are shifted 60 electrical degrees. Upon loss of a phase, adjacent phases share the load on the missing phase and current peak values increase significantly. As this is not a three-phase machine, it does not stop and continues producing torque. Stator current trajectory shows a current drop in the direction of the lost phase and increment in orthogonal direction.

Experimental results of steady state stator currents are shown in Fig. 1 and Fig. 2. Here stator phase F is open.

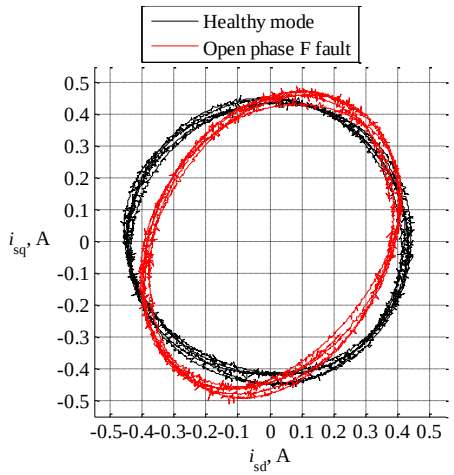

Fig.1. Stator current trajectory in healthy mode and under open phase F fault condition without adjustments

While the mean power consumption stays the same, stator current trajectory and, therefore, the flux trajectory becomes elliptical (Fig. 1) in faulty mode.

Effective stator phase current values in healthy mode are equal and in faulty mode (Fig.2) they are all different in an induction motor with an isolated neutral point. The effective value in the greatest phase current is 40 % greater in faulty mode (correspondingly 92,4 mA and 129 mA).

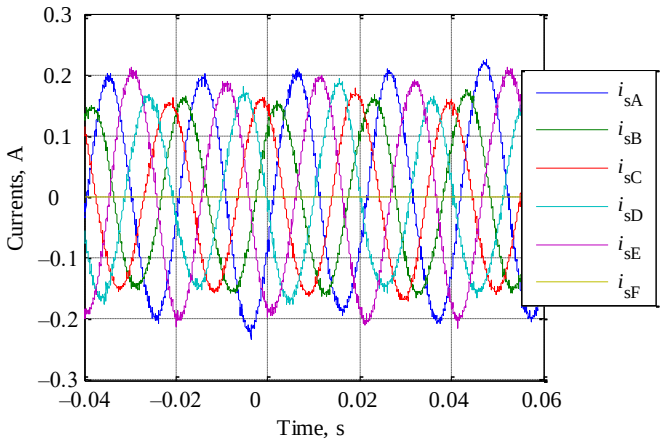

Fig.2. Steady state currents under open phase F fault condition without adjustments

III. CONTROL OF STATOR CURRENTS BY ADJUSTING STATOR VOLTAGE ANGLES

Adjusting the angles of voltage phases generated by inverter is proposed as a method for control of current trajectory in stator phase fault mode. This way meeting the minimum copper loss criterion is expected.

In healthy mode the six stator voltage phase angles are 0°, 60°, 120°, 180°, 240°, 300°. In faulty mode F phase (the 300°) is open and, therefore, adjustments to adjacent phases are made.

Drawing the adjacent voltages closer to the lost F, 10° and 20° are tried and the results are shown in Fig. 3. Here the angles of phases A to E are 350°, 60°, 120°, 180°, 250° and 340°, 60°, 120°, 180°, 260° for 10° and 20° shifts correspondingly.

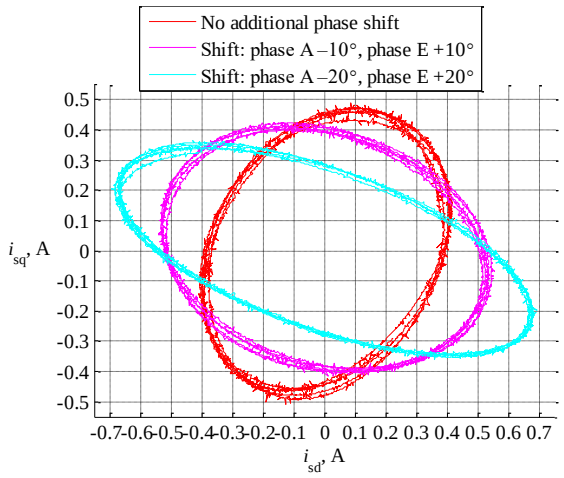

Fig.3. Stator current trajectory under open phase F fault condition with adjustments: additional phase A shift of -10° and phase E shift of +10; and additional phase A shift of -20° and phase E shift of +20°

Based on trajectories presented in Fig. 3, it is obvious that a more circular stator current trajectory could be achieved using the proposed method. Although there is a 60° angle between stator current vectors, a 10° voltage angle shift of two phases is two phases is too great.

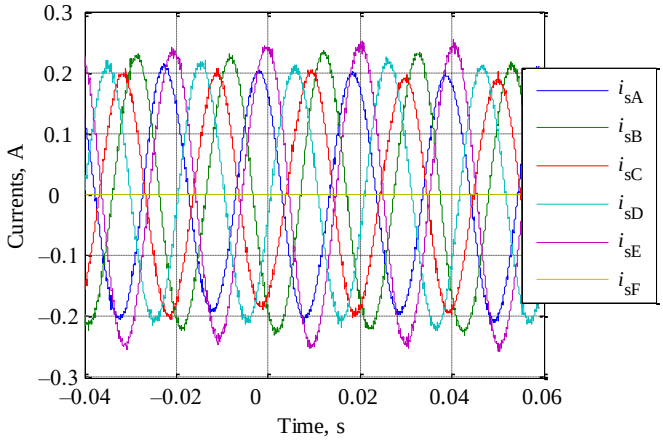

Fig.4. Steady state currents under open phase F fault condition with additional phase A shift of -10° and phase E shift of +10°

Voltage phase adjustments in both cases had a negative effect on instantaneous currents: peak values increased significantly in most phases. Note that shift in current phase angles does not match voltage angles. Current phase angle shifts in A and E phases are 40–50° instead of 10°. This effect would not be present in an induction machine with a grounded neutral point.

IV. REDISTRIBUTION OF STATOR CURRENTS

By running multiple experiments with various stator voltage angle shifts, a near circular current trajectory was achieved (Fig. 5).

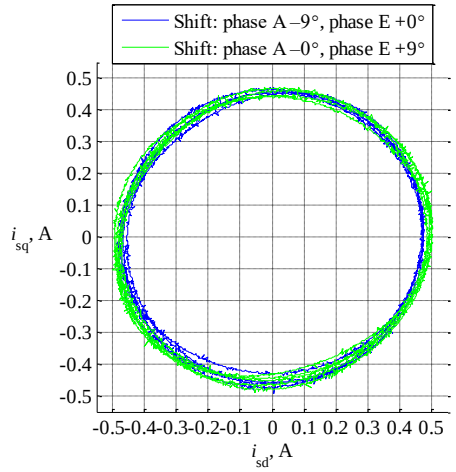

Fig.5. Stator current trajectory under open phase F fault condition with adjustments: additional phase A shift of -9° and phase E shift of +0°; and additional phase A shift of -0° and phase E shift of +9°

The most important conclusion to be made is that optimal (circular) trajectory can be achieved with numerous phase shifts and does not have a sole solution. Analysis of instantaneous stator phase currents is in order.

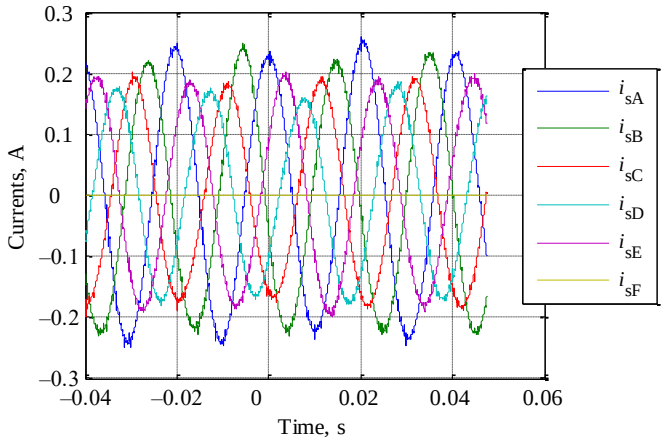

Fig.6. Steady state currents under open phase F fault condition with additional phase A shift of -9°

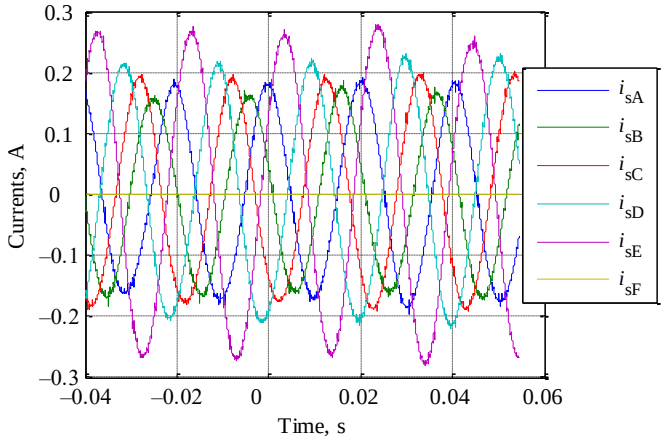

Fig.7. Steady state currents under open phase F fault condition with additional phase E shift of +9°

In Fig. 6 and Fig. 7 instantaneous stator phase currents are presented for both angle shifts. Both cases show worse results compared to unadjusted open-phase fault mode as peak values are significantly greater in some phases (Fig. 2): 62% and 81% correspondingly compared to 40% of unadjusted faulty mode. This would cause a significant strain on all of the system as it might result in further damage.

Note that greatest currents flow in different phases (Fig. 6 and Fig. 7). This means our method allows any distribution of power to all phases. The optimal redistribution would uniform currents of all the stator phases. This way minimum copper loss criterion would also be met.

The best result was achieved by changing 4 phase angles (Fig. 8). Note that the minimum stator voltage angle shift increment is 1°.

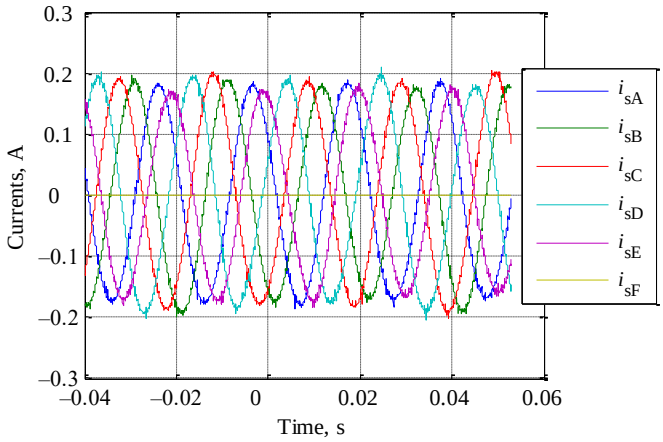

Fig.8. Steady state currents under open phase F fault condition with additional phase A shift of -6°, phase B shift of -1°, phase D shift of +4° and phase E shift of +6°

The achieved effective value in the greatest phase current is 31 % greater in adjusted faulty mode while in the unadjusted mode it is 40 % (Fig. 8).

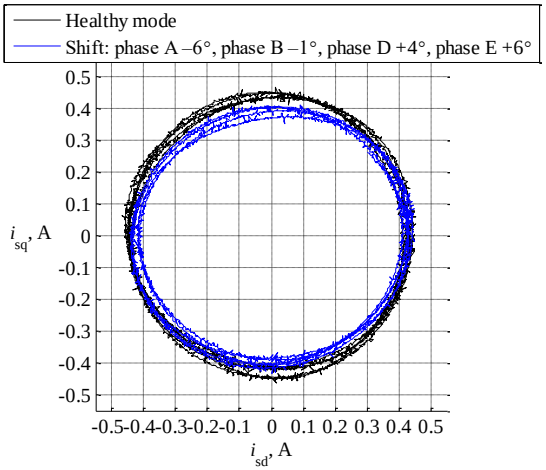

Fig.9. Stator current trajectory under open phase F fault condition with additional phase A shift of -6°, phase B shift of -1°, phase D shift of +4° and phase E shift of +6°

The stator current trajectory is slightly more elliptical compared to results presented in Fig. 5. This is considered to be the best result as the over-all quality was increased.

Mathematical model of an asymmetric induction machine is

not accurate enough to reproduce experimental results. Stator phase voltage angles are adjusted by 10% to achieve near circular current trajectories. This degree of accuracy could not be guaranteed.

V. Conclusion

A compensation method for stator open-phase fault is presented. It allows control of stator current amplitudes by adjustment of stator voltage phase angles without reducing voltage amplitudes. This way maximum potential is drawn from the power source and no investments or changes to the hardware are required.

Using proposed method circular stator trajectory can be achieved. Experiments show that slight adjustments to voltage phase angles (up to 10% of spatial displacement of adjacent stator windings) has great impact on the trajectory in an induction motor with isolated neutral point. Currently mathematical models are not accurate enough to calculate optimal stator voltage phase angles with required accuracy.

Individual stator phase currents can also be controlled. One of the currents increases 40% during open-phase fault compared to healthy mode which may cause damage to the machine. With a minimal stator phase angle shift increment of one degree the greatest current was reduced to 31%. In theory, equal effective stator current values of all phases may be achieved with optimal stator voltage phase angles and, therefore, the greatest current value could go down to 20%.

In all modes, including the healthy mode, power consumption is almost the same.

References

[1] D. Foito, J. Maia, V. Fernao Pires, J. F. Martins, “Fault diagnosis in six-phase induction motor using a current trajectory mass center”, Measurement, Vol. 51, May 2014, pp. 164-173.

[2] A. Nanoty, A. R. Chudasama, “Control of designed developed six phases induction motor”, International Journal of Electromagnetics and Applications, Vol. 2, 2012, pp. 77-84.

[3] A. Nanoty, A. R. Chudasama, “Design, development of six phase squirrel cage induction motor and its comparative analysis with equivalent three phase squirrel cage induction motor using circle diagram”, International Journal of Emerging Technology and Advanced Engineering, Vol. 3, Iss. 8, August 2013, pp.731-737.

[4] G. Grandi, A. Tani, P. Sanjeevikumar, D. Ostojic, “Multi-phase multi-level AC Motor drive based on four three-phase two-level inverters”, International symposium on power electronics electrical drives automation and motion, 2010, pp. 1768-1775.

[5] R. Gregor, F. Barrero, S. L. Toral, M. J. Duran, M. R. Arahal, J. Priesto, J. L. Mora, “Predictive-space vector PWM current control method for asymmetrical dual three-phase induction motor drives”, IET Electric Power Applications, Vol. 4, Iss. 1, 2010, pp. 26-34.

[6] P. Nagaraj, V. Kannan, M. Santhi, “Modified multiphase induction motor with high starting torque”, International journal of Innovative Research in Science, Engineering and Technology, Vol. 3, Iss. 3, March 2014, pp. 519-522.

[7] M. J. Duran, I. Gonzalez, M. Bermudez, F. Barrero, H. Guzman, M. R. Arahal, “Optimal fault-tolerant control of six-phase induction motor drives with parallel converters”, IEEE transactions on industrial electronics, 2015.

[8] H. Guzman, I. Gonzalez, F. Barrero and M. Durán, R. Gregor (Ed.), “Open-Phase Fault Operation on Multiphase Induction Motor Drives, Induction Motors - Applications, Control and Fault Diagnostics”, InTech, November 2015.

[9] P. S. Bhowmik, S. Pradhan, M. Prakash, “Fault diagnostic and monitoring methods of induction motor: a review”, International Journal of Applied Control, Electrical and Electronics Engineering, Vol.1, iss. 1, May 2013.

Biographies

AURELIJUS PITRĖNAS is a Ph.D. student at the department of Automation of Vilnius Gediminas Technical University (Lithuania) and works as an assistant in Vilnius Gediminas Technical University. He graduated B.S. and M.S. degrees in electrical engineering, Vilnius Gediminas Technical University in 2010 and 2012 respectively.

Research interests: automated control systems, embedded systems, power electronics.

DONATAS UZNYS was born in Lithuania, Klaipeda city, in 1988. He received the B.S. and M.S. degrees in electrical engineering from the Vilnius Gediminas Technical University, Vilnius, in 2010 and 2012 respectively and is currently working on his Ph.D. thesis in electrical engineering.

Since 2012, he has been an Assistant with the Department of Automation, Vilnius Gediminas Technical University. His research interests include induction motor drives, computer modelling and fuzzy logic.

DOMINYKAS BEIŠTARAS is a Ph.D. student at the department of Automation of Vilnius Gediminas Technical University (Lithuania). He received the B.S. and M.S. degrees in electrical engineering from the Vilnius Gediminas Technical University, Vilnius, in 2012 and 2014 respectively.

Research interests: system identification and optimization, induction motor drives.

Some Features of Computer Simulation Transitional Processes at Switching-off Unloaded Transformers

T. Lazimov, A. Sadigov, and Sh. Mammadly

***Abstract*— Stability of computer simulation transitional processes at switching-off unloaded power transformers is considered in the article. Solvability and stability of solutions of this problem had been tested by the four stiff ordinary differential equations' solvers in the wide ranges of initial step sizes and relative tolerances. On the base of analyze the calculated values of voltages across the terminals of switched-off transformer and recovery voltage across the poles of circuit-breaker there were made some conclusions and stated the features of the simulation process. Results at use both fast and robust algorithms of the ode solvers were analyzed and compared in the article.**

Index Terms— **fast and robust algorithms, initial step size, ordinary differential equations' solvers, relative tolerance, stability of solutions.**

I. Introduction

As it is known the most dangerous switching transients from the point of view the transitional voltages' magnitudes take place at switching-offs small inductive currents of unloaded transformers and autotransformers and capacitive currents of power capacitor banks and unloaded no-load power transmission lines [1], [2].

Numerical modeling and computer simulation being the main way to study transitional processes in power electric systems have usually faced with the necessity to provide stability of solutions because that these problems relate to the so called "stiff" ones [3]. Successful computer simulation (in other words, getting the stable solutions) of this class of problems requires determination of appropriated ordinary differential equations' solvers (ode solvers) and optimal simulation parameters i.e. initial step sizes an relative tolerance [4].

We had previously got some results in the area under consideration. Recall them briefly.

T. LAZOMOV, Electric Supply and Insulation Chair, Azerbaijan Technical University, AZ 1073, Baku, Azerbaijan (e-mail: tahirlazim@gmail.com)

A. SADIGOV, Electric Supply and Insulation Chair, Azerbaijan Technical University, AZ 1073, Baku, Azerbaijan (e-mail: sadiqov.abzk@mail.ru)

Sh. MAMMADLY, Electric Supply and Insulation Chair, Azerbaijan Technical University, AZ 1073, Baku, Azerbaijan (e-mail: sefiqe_mdm@mail.ru)

Manuscript received August 23, 2016; accepted October 17, 2016.
DOI: 10.17694/bajece.292577

There was stated in [5,6] that there is a notable dependence of stability on the simulated network parameters, especially free frequencies and damping factor. The worst stability takes place as a rule for the higher free frequencies. Note in this view that there are at least 2 important features complicating computer simulation the problem under consideration, namely:

- relatively high free frequency at unloaded transformers switching-off conditioned by the very little values of their input capacitance equaled to units and tens of nanofarad;
- a steep rise of electrical strength's restoration law in the initial period of contacts separation taken place for vacuum circuit-breakers.

Both features lead to increasing of a global error of simulation via increasing the local errors with evident possible impact on stability.

As it may be assumed increasing of damping will lead to improving of stability. It may be done on the base of general suppositions concerned to physical and computational nature of the problem considered. But as we stated in [3] assumption on positive influence of damping on the stability of solutions is not so evident.

In the present article stability of solutions at computer simulations of unloaded transformers switching-off is studied in details.

II. Computational Ground and Conditions

Multi-phase induction motors are used in wind power systems, electrical and hybrid vehicles [5], electric ship propulsion [6], in 'more electric aircraft' actuators and in safety-critical applications, such as aerospace or military naval drives, where fault tolerance is a desirable feature [7].

Theoretical and computational ground of the problem considered is presented on some our previous works, e.g. [3], [7-9]. The equivalent schemes and switching-off conditions are given in [3,5-7]. The laws of restoration electrical strength of circuit-breaker (in other words the function of breakdown voltage of inter-contact space of circuit-breaker) are offered and analyzed in [9-11].

The stiffness of differential equations in relation to network parameters and stability problem at computer simulation transitional switching-offs in electric power systems were considered in [3,5,8] and some other works.

The present research was dedicated to study of stability at computer simulation switching-offs unloaded power transformer of rated voltage 110 kV and rated apparent power

32 MVAr. The transformer is switched by the vacuum circuit-breaker with electrical strength restoration law given in [9].
The numerical methods ode 23s, ode 23tb, ode 23t and ode 15s included to the Simulink ode Solvers were used for computer simulation. The MATLAB r2013a version was used for simulation.

III. Discussion

Let us now consider the results of computer simulation at use so called stiff solvers ode 23s, ode 23t, ode 23s and ode 15s included to the Simulink-MATLAB set.
Fig.1 presents graphs of transitional voltages across the switched-off transformer's high-voltage terminals got at use all the above-minded ode solvers for initial step sizes varied between 10 nanoseconds and 100 microseconds and tolerances between 10^{-6} and 10^{-4}. Fig.2 presents graphs of transitional recovery voltages at use the same methods and simulation parameters. The robust algorithms were used. As it is seen from the Fig.1 and Fig.2 the solver 23s and all the robust algorithms of the ode 23t, ode 23tb and ode 15s provide good solvability and stability of solutions both for the functions of voltage across the switched-off transformer's high-voltage terminals and recovery voltage (i.e. voltage across the circuit-breaker's poles). The most deviations from the transitional voltages' stable values in the given ranges of simulation parameters do not exceed 4 percent for the voltage across the terminals (V) and 1 percent for the recovery voltage (ΔV). For both functions' graphs of the transitional functions against the initial step size are successfully converge to their stable values.

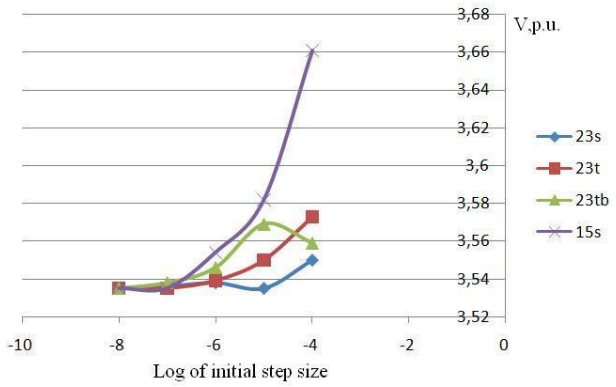

Fig.1. Calculated voltage ratios against initial step size at use robust algorithms (relative tolerance 0.000001)

Fig.3 and Fig.4 present graphs of transitional voltages across the switched-off transformer's high-voltage terminals and transitional recovery voltages respectively got at use the fast algorithms of above-minded ode solvers for initial step sizes varied between 10 nanoseconds and 100 microseconds and tolerances 10^{-6} and 10^{-4}.

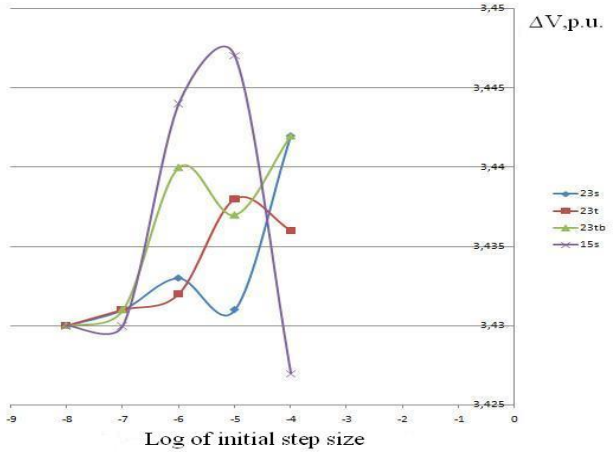

Fig.2. Calculated recovery voltage ratios against initial step size at use robust algorithms (relative tolerance 0.000001)

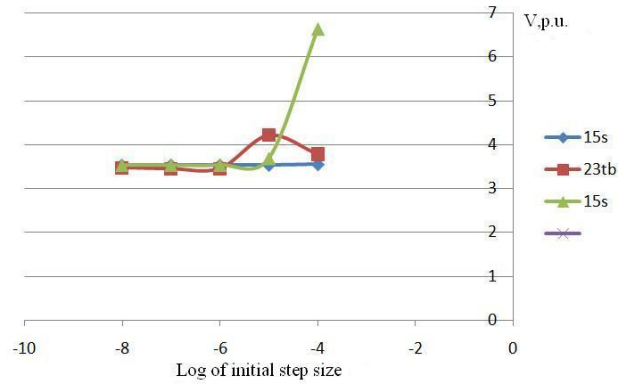

Fig.3. Calculated voltage ratios against initial step size at use fast algorithms (relative tolerance 0.000001)

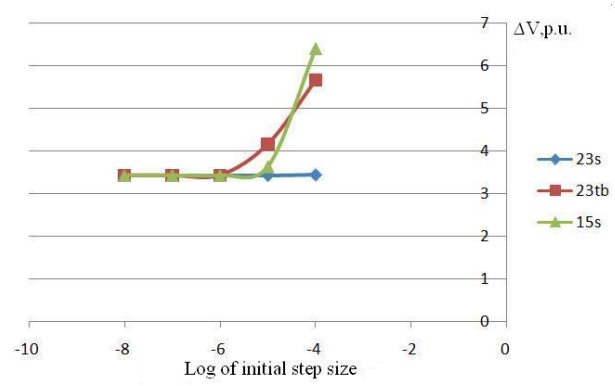

Fig.4. Calculated recovery voltage ratios against initial step size at use fast algorithms (relative tolerance 0.000001)

As we can see from these figures the fast algorithms have notable worse solvability and stability comparatively with corresponding robust ones. Thus, the fast algorithm of the ode 23t solver does not provide stability of solutions and is characterized

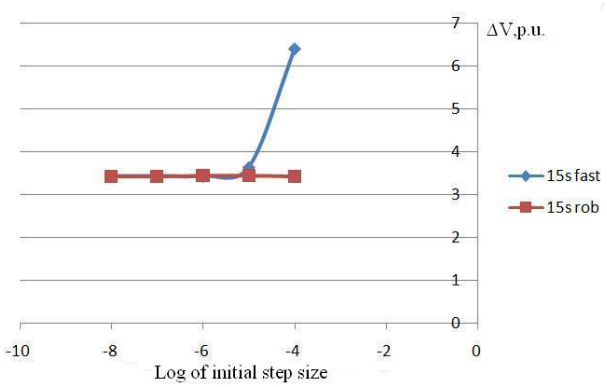

Fig.5. Comparison of calculated recovery voltage ratios at use robust and fast algorithms (relative tolerance 0.000001)

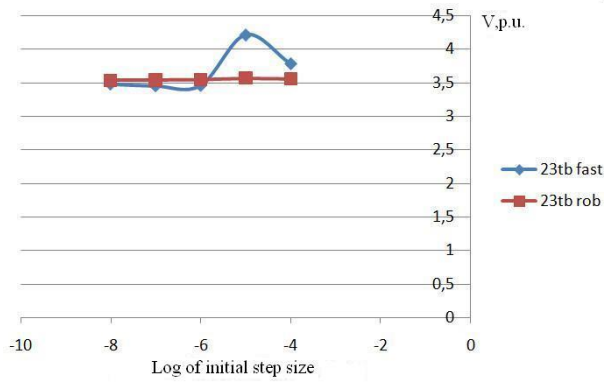

Fig.6. Comparison of calculated voltage ratios at use robust and fast algorithms (relative tolerance 0.000001)

with very big deviations from the stable solutions. The fast algorithm of the 23tb method has much better solvability but does not provide reaching of stability even at the least simulation parameters (initial step size 10 nsec and relative tolerance 10^{-6}).

For the more explicit demonstration of behavior of solutions at use the fast and robust algorithms is used comparative presentation of graphs of the transitional functions against the initial step size given in Fig.5 for the recovery voltage (ode 15s solver) and in Fig.6 for the voltages across the switched-off transformer's high-voltage terminals. As it is seen from the Fig.5 there is great difference (deviation from the stable solution) between the values of transitional voltages calculated with use the different algorithms (the fast and robust ones) of the same solver, i.e. ode 15s in the considered case. In the same time there has taken place rapid convergence of the calculated transitional functions against initial step size which stabilize beginning from the relative tolerance 10^{-4}. But in some cases transitional function calculated at use fast algorithm cannot reach its stable value got at use the appropriate robust algorithm even for very little given values of the relative tolerance (see Fig.6). As a rule further decreasing of the relative tolerance leads to significant increasing of simulation time.

IV. Conclusions

The ode 23tb and 23t solvers have no solvability for the fast algorithm. Both solvers have good solvability and convergence for the robust algorithm especially at the initial step size no more than 10^{-5} sec and relative tolerance no more than 10^{-5}.

The ode 23s solver (having no robust algorithm) demonstrates good solvability and convergence at simulation the problem under consideration in given ranges of initial step size (between 10 nsec and 100 μsec) and relative tolerance (between 10^{-6} and 10^{-4}).

The ode 15s solver demonstrates good solvability and convergence for the robust algorithm especially at the initial step size no more than 10^{-6} sec and relative tolerance no more than10^{-4}. Worse (but satisfactory) solvability and convergence have taken place for the fast algorithm at the initial step size no more than 10^{-6} sec and relative tolerance no more than 10^{-4}. Note that the value of tolerance 10^{-4} is satisfactory just at the least values of the initial step size i.e. 10 nsec.

References

[1] D.V. Razevig, High Voltage Engineering, Khanna Publishers, 1972.

[2] J.P. Bickford, N. Mullineux, S.R. Reed, Computation of Power Systems Transients, Peter Peregrinus Ltd, England, 1976.

[3] T. Lazimov, E. Saafan, "Influence of Arc Resistance on Transitional Functions' Stability at Computer Simulation of Switching-off Processes", Proc. of the IEEE PES APPEEC Conference, Hong-Kong, 2014, pp. 1-4.

[4] L. F.Shampine, Numerical solutions of ordinary differential equations, Chapman and Hall, New-York, 1994.

[5] T. Lazimov, S. Imanov, "On stability while simulating the switching-offs the capacitive and small inductive currents," in Proc. 2006 of MEPS International Symposium, Wroclaw, Poland, pp. 407-410.

[6] T. Lazimov, E. Saafan, "On interaction between circuit-breaker and network at small inductive currents' switching-offs," Present Problems of Power System Control, Wroclaw, Poland, vol. 1, pp. 23-31, 2011.

[7] T. Lazimov, S. Akhundov, "Research on Influence of High-Voltage Circuit Breakers' Characteristics on Switching Overvoltages and Overcurrents," in Proc. 2003 of the III International Conference ELECO, Bursa, Turkey, pp. 1-4.

[8] T. Lazimov, S. Akhundov, "Peculiarities of transients' simulation in electrical circuits," in Proc. 2003 of the Republican Conference on IT, Baku, Azerbaijan.

[9] H. Mammadov, T. Lazimov, S. Imanov, "Improved model of circuit-breaker's dielectric strength restoration," in Proc. 2009 of the ELECO International Conference on Electrical and Electronic Engineering, Bursa, Turkey, pp. 354-356.

[10] T. Lazimov, S. Akhundov, "Modeling of electrical strength of high voltage circuit-breakers," in Proc. 2001 of the International Symposium SIEMA, Kharkov, Ukraine, pp. 112-114.

[11] T. Lazimov, S. Imanov, E. Saafan, "Transitional Recovery Voltages at Capacitive Currents Switching-off's by Vacuum and SF6 Circuit-Breakers," in Proc. 2010 of MEPS International Symposium, Wroclaw, Poland, pp. 777-783.

Biographies

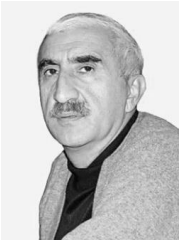

Tahir LAZIMOV was born in Baku, Azerbaijan in 1955. He received the engineer qualification in electrical engineering from the Azerbaijan State Oil Academy, Baku, in 1977, Ph.D. degree in high voltage engineering from the Tomsk Polytechnic Institute, Tomsk, Russia Federation, in 1989 and D.Sc. degree in electrical engineering from the Azerbaijan Power Engineering Institute, Baku, in 1997. He has been a Professor since 2006 (Presidential Higher Attestation Commission).

From 1977 to 2004 he worked in the Power Engineering Research Institute, Baku, where he occupied the positions of Academic Secretary and Principal Researcher.
Since 2004 he has been a head of the Electric Supply and Insulation Department in the Azerbaijan Technical University, Baku. He is the author of about 180 scientific works including five books, dozens of articles and papers published in scientific journals and transactions and International conferences' proceedings, methodical works and inventions. His research areas include transitional processes in power electric systems and their computer simulation, power systems electromagnetic compatibility. Ph.D. and M.Sc. thesis are preparing under his supervision.
Professor T. Lazimov is IEEE Senior member, the member of the Scientific Board on Technology at the Azerbaijan National Academy of Science and also some other scientific councils and editorial boards in Azerbaijan and abroad.

Asif SADIGOV was born in Baku, Azerbaijan in 1993. He received the Bachelor of Science and Master on Science degrees on Electrical Power Engineering in 2014 and 2016 respectively, both from the Azerbaijan Technical University.
He has occupied the engineer position in the "Electric Supply and Insulation" chair of the Azerbaijan Technical University since 2015.
His research areas include transitional processes in power electric systems and their computer simulation.

Shefiga MAMMADLY was born in Baku, Azerbaijan in 1994. She received the Bachelor of Science degree on Electrical Engineering in 2015 from the Azerbaijan State Oil and Industry University.
Presently she is a Master student on Electrical Power Engineering at the "Electric Supply and Insulation" chair of the Azerbaijan Technical University. Her master thesis is devoted to study of stability at computer simulation of switching processes in high-voltage electric power systems.

Wireless Hand Rehabilitation System (WHRS)

A.Gücüyener, and E. Kaplanoğlu

***Abstract*—Loss of motor skills in hand due to several reasons affects daily life in a negative way. Treatment or rehabilitation must be applied in order to reactivate motor skills. Different systems were developed in the rehabilitation process by benefiting from technology. Those systems work as telerehabilitation-based or with external skeleton manipulator. An internet connection is required for telerehabilitation-based systems and a physical therapist must carry out the rehabilitation process for systems with external skeleton manipulator. This shall increase the work load of physical therapist. In this study, it is aimed to decrease the work load of physical therapist and develop a hand rehabilitation system with easier and more flexible usage. With this purpose, a system that consists of three units communicate with each other wirelessly and which could be used even without a physical therapist.**

Index Terms—**Rehabilitation hand, wireless control, mobile rehabilitation, wearable rehabilitation devices.**

I. Introduction

Loss of motor skills in hand occurs as a result of, hemiplegia, neurotic diseases or muscular diseases. That loss is also a medical problem which affects human life in a negative way. A surgical or medical intervention shall be required. Before or after those interventions, hand rehabilitation shall be applied in order to re-function motor skills that are already lost.

Hand rehabilitation is a process which includes assessment and rehabilitation of hand. Traditional methods could be used during the assessment process. But, for the rehabilitation process, several rehabilitation systems are developed as an alternative for traditional methods.

When those rehabilitation systems that could be used in hospitals or physical therapy centers are reviewed; it is seen that systems that shall decrease the work load of physical therapist [1, 2] or that shall increase the participation of the patient to the rehabilitation process [3, 4] are developed. It could be said that those systems are with external skeleton manipulator [5] or tele-rehabilitation based [6]. Those systems, which are developed in order to decrease work load of physical therapist, are generally operated remote-controlled based [7].

A. GÜCÜYENER, Department of Electronic Technology, Vocational School, Istanbul Arel University, Istanbul, Turkey, (e-mail: aytekgucuyener@arel.edu.tr).

E. KAPLANOĞLU, Department of Mechatronics Engineering, Technology Faculty, University of Marmara, Istanbul, Turkey, (e-mail: ekaplanoglu@marmara.edu.tr).

Manuscript received June 5, 2016; accepted September 17, 2016.
DOI: 10.17694/bajece.292651

There must be an internet connection where the patient uses the system in order to remote control the system [7]. Systems with external skeleton manipulator could not be used in the hand assessment process since they are designed for forcing the patient to make a certain movement.

In the Wireless Hand Rehabilitation System (WHRS), it is aimed to make the rehabilitation process independent from hospital and physical therapist. Accordingly, rehabilitation process is turned to an autonomous system. Hand figures, which physical therapist could determine and arrange, are included in WHRS. Thus, hand figures for practices could be performed by the system without an internet connection. Physical therapist could make a tailor-made prescription for the patient by changing practice figures as he likes.

Before system shall be used, practice prescription to be used must be loaded to the system by physical therapist. After system is operated, it makes an application report by using the prescription which is determined by physical therapist and the numbers of repetition.

By means of records which is kept during the time when WHRS is used, it is possible to analyze practices of patient and to reform the rehabilitation process due to this analysis.

Since units in the system could communicate wirelessly, it provides more flexible usage for the patient. Patient could use WHRS wherever he likes.

II. Specifications of WHRS

That system actualizes rehabilitation process by simulation. The system consists of a “robot hand” for the patient to see the practice figure, a “data glove” to read data in the figures which are made by patient and a “control center” which ensures all those units work together. While hand rehabilitation firstly, Robot Hand Unit is realized posture/grasp which is planned from physiotherapist then patient try to make this posture/grasp with Data Glove Unit. All data from glove hand unit is recorded by control center unit. Those units communicate with each other wirelessly. XBee S2 RF module is used in order to allow units to communicate wirelessly with each other [8]. Units in the system are all shown in Fig.1.

Fig. 1 Wireless hand rehabilitation system. (1) robot hand unit, (2) control center unit, (3) data glove unit

A. *Data Glove Unit*

Data Glove Unit consists of a glove, 6 pieces of flex sensors [9, 10], a control card with ATmega328P microcontroller [11] and XBee S2 RF wireless module [8]. A system with microcontroller is formed for flex sensors and wireless communication module in Data Glove in order to work together. Wiring diagram of microcontroller with other units is shown in Fig.2. The unit must send practice information of the patient to the Control Center.

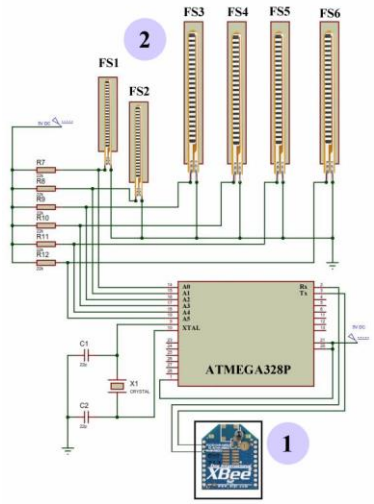

Fig. 2 Data glove unit connections. (1) rf module, (2) flex sensors

Values shown in Table 1 are measured by flex sensors in Data Glove.

TABLE I
FLEX SENSOR'S VALUE

Analog Read	In_min	In_max	Out_min	Out_max
FS1 (A0)	515	600	5	175
FS2 (A1)	665	680	5	175
FS3 (A2)	290	500	5	175
FS4 (A3)	335	520	5	175
FS5 (A4)	315	510	5	175
FS6 (A5)	270	460	5	175

Flex sensor values in Table 1 are turned to motor angle values by using map function [12] in Eq. (1).

$$mf = (FS(i) - IN_{min}) * \frac{(OUT_{max} - OUT_{min})}{(IN_{max} - IN_{min})} + OUT_{min} \quad (1)$$

B. *Robot Hand Unit*

The unit consists of a prototype hand that is made by printing from a 3-D printer, 6 pieces of servo motor in order to apply finger angles to that hand [13], XBee S2 RF module [8] for wireless communication and ATmega328P microcontroller [11] which shall control the unit itself.

In the robot hand, which consists of 17 parts in total, joints are made of springs that are hanged by pins. After joints are completed, nylon thread connected to 6 servo motors goes through joint channels and connected to fingertips in order to provide flexion and extension for fingers. Servo motors and wireless communication module that are used in Robot Hand unit are controlled by a system with microcontroller. The connection of this microcontroller with other units is shown in Fig.3.

V1 thumb is used in order to provide abduction and abduction movement. Servo motors named V2-V6 provide flexion and extension movement for relatively thumb, fore finger, middle finger, ring finger and little finger. While flexion is provided by servo motors in all fingers, extension movements of fingers are supported with springs.

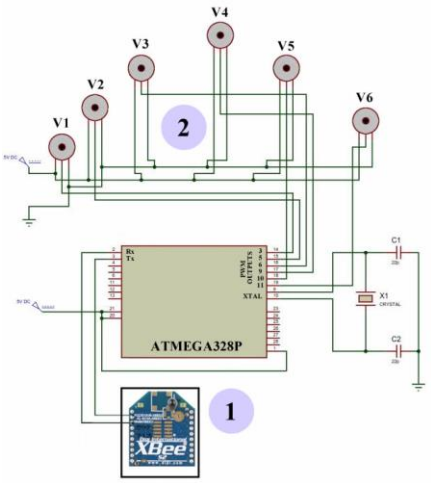

Fig. 3 Robot hand unit connections. (1) rf module, (2) servo motors

C. *Control Center Unit*

This unit consists of a touchscreen [14], real-time time module [15], XBee S2 RF [8] module and wireless SD extension port [16] and an ATmega2560 [17] microcontroller in order to control the unit. Microcontroller communicates with touchscreen via a serial port. System is controlled in line with messages coming from touchscreen. Content and repetition information in the memory card are read by the microcontroller and an application table shall be made. Wiring diagram of the unit is shown in Fig.4.

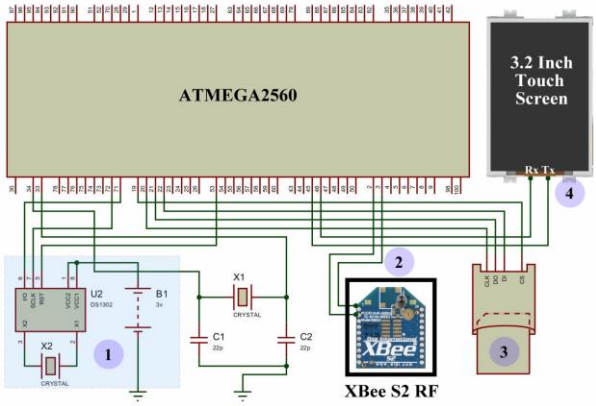

Fig. 4 Control center unit connections. (1) real time clock module, (2) rf module, (3) memory card module, (4) touch screen.

D. *Wireless Network*

In that system, XBee S2 RF modules in Data Glove and Robot Hand Units are configured as director. They are also configured as coordinator in Control Center unit. Those three modules are examined and tested by connecting to a computer without integrating the network that they form. Identity called "2015" is determined as PAN ID. Physical address of the coordinator is recorded in the directors and the network is formed in Fig.5 where they could communicate with each other. Message no.1 in Fig.5 is used to control the communication. Control Center unit sends "CR!" and "CG!" messages to the network. When message "OKR!" from Robot Hand Unit and message "OKG!" from Data Glove Unit are receives, it is understood that there is no problem in the communication. Message no.2 in Fig.5 states messages between Control Center and Robot Hand. Control Center sends a new figure to Robot Hand. Robot Hand performs that figure and send "OKR!" message. Message no.3 in Fig.5 states messages between Control Center and Data Glove. Control Center sends "DG!" message. Data Glove sends the data obtained by measuring the value starting with "DGE!" from flex sensors in the map function to Control Center Unit.

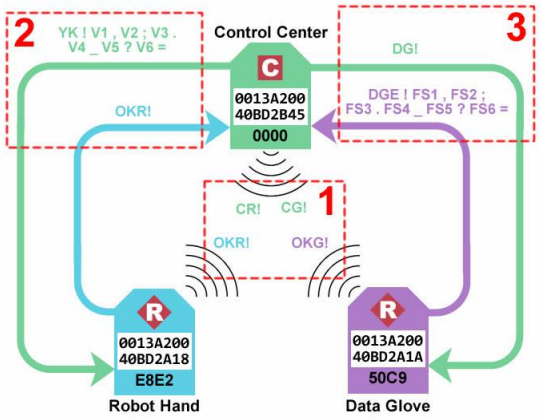

Fig. 5. Structure of the wireless network (1) communication control of WHRS (2) control center unit communication with the robot hand unit (3) control center unit communication with the data glove unit

III. SOFTWARE ARCHITECTURE OF WHRS

Generally, the operating logic of the system is to include the prescription to be applied with a memory card stick in the Control Center in the system itself. Due to touchscreen in Control Unit, tolerance and time values could be determined by user with the help of menus with Turkish and English language options. After practice information in the memory card shall be sent to the Robot Hand Unit, Robot Hand unit performs this practice. Patient who shall use the system shall also wear that glove on his hand and tries to do the same practice. At the same time, there shall be some visual messages giving information to the user are shown on the screen. Residual time and instant finger angles are shown on the screen. While system is being operated, finger angle information from Robot Hand and Data Glove shall be compared and results shall be recorded to the memory card in the Control Center. Mathematical transactions in Eq. (5) and (6) shall be used in that comparison transaction.

$$rh_i \rightarrow 5 \leq rh_i \leq 175 \tag{2}$$

$$dg_i \rightarrow 5 \leq dg_i \leq 175 \tag{3}$$

$$z = rh_i * tolerance \tag{4}$$

$$f(i) = \begin{cases} 1, & if \quad rh_i - z \leq dg_i \leq rh_i + z \\ 0, & if \quad rh_i - z \geq dg_i \; or \; dg_i \geq rh_i + z \end{cases} \tag{5}$$

$$Compare = \begin{cases} Succeed, & if \sum_{i=1}^{6} f(i) = 6 \\ Fail, & if \sum_{i=1}^{6} f(i) \neq 6 \end{cases} \tag{6}$$

If the user could complete the practice successfully, then that information shall be recorded as successful in the memory card. If user could not perform the practice within the time range, then system shall record this as an unsuccessful attempt and pass to the other practice. Software algorithm of WHRS is shown in Fig.6.

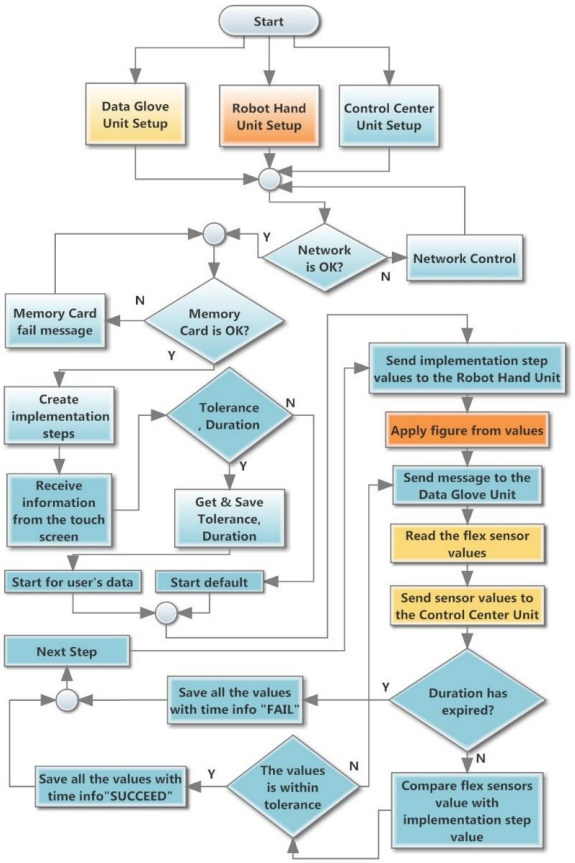

Fig. 6. System algorithm

IV. CASE STUDIES

When WHRS is operated, first the name of the application shall be formed in Robot Hand Unit and that shall be compared with values from Data Glove unit. Both successful

and unsuccessful record examples are shown in Fig.7 for an example figure.

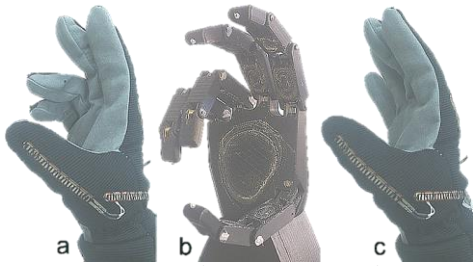

Fig. 7 Case Study (a) succeed figure (b) original figure (c) fail figure

In Fig.7, two example studies are taken into consideration for the same figure. In the Example A, since all fingers are within the tolerance range, it shall be deemed successful. In Example B, since 5th and 6th values are out of the tolerance range, this shall be recorded as unsuccessful/failed study. Those values are shown graphically in Fig.8.

Application values at the moment when system is being used shall be kept and recorded in a file called "results.csv" in the memory card. As you could see in Table 2, number of steps, date, time, tolerance and arranged time information in the application table of the system are added to "results.csv" file. RH1 and DG1 values are parts where related data of Robot Hand Unit and Data Glove are compared with each other. It is deemed that the value from Robot Hand Unit has a surplus of missing in the amount of tolerance value.

After all practices are completed, user shall give the memory card which includes all details about practices to the physical therapist. Physical therapist could see all details that which practices could be made by user or not with the information on time and date. If physical therapist finds necessary, he could update the system by removing those practices which are already done and by adding new practices. Physical therapist could apply different practices to different patients with the same system.

TABLE II
THE RESULTS AFTER USING THE SYSTEM

Step	Date	Time	Tolerance	SetTime	Sec	RH1	DG1	RH2	DG2	RH3	DG3	RH4	DG4	RH5	DG5	RH6	DG6	Result
1	15.12.2015	15:40	30	60	54	40	39	175	175	175	175	175	175	175	175	175	175	Succeed
2	15.12.2015	15:42	30	60	0	50	45	10	175	10	28	10	18	10	21	10	24	Fail
3	15.12.2015	15:52	30	60	29	40	31	175	175	175	163	175	175	175	166	175	175	Succeed
4	15.12.2015	16:00	30	60	39	120	136	100	90	12	15	12	14	80	72	80	70	Succeed

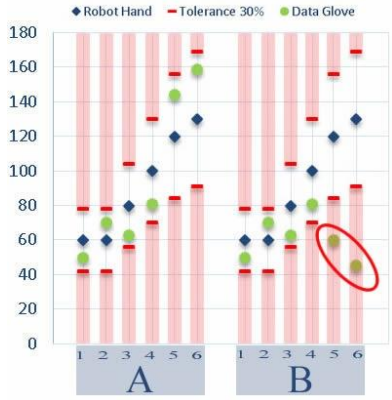

Fig. 8 case study of the comparison operation (a) succeed figure (b) fail figure

V. CONCLUSIONS

In this study, a system which operates hand rehabilitation procedure autonomously and independent from physical therapy center and physical therapists. Due to this system, patient could use hand rehabilitation process wherever he likes without any need for internet connection. Also, those units which communicate wirelessly with each other provide flexible usage.

VI. FUTURE WORK

System is made for only right hand. A Data Glove for left hand shall be made and this new glove shall be used in a rehabilitation center and results shall be reviewed.

It is considered to add multi-user function to the system by applying the system to more than one patient who have same diseases.

REFERENCES

[1] Zhang, S., Guo, S., Gao, B., Hirata, H., Ishihara, H.,(2015), "Design of a novel telerehabilitation system with a force-sensing mechanism.", Sensors, Vol.15, pp. 11511-11527, ISSN: 14248220, (Switzerland).

[2] Durfee, K. W., Weinstein, A. S., Carey, R. J., (2005), "Home stroke telerehabilitation system to train recovery of hand function", 9th International Conference on Rehabilitation Robotics, pp.353-356

[3] Pyk, P., Wille, D., Chevrier, E., (2008), "A Paediatric Interactive Therapy System for Arm and Hand Rehabilitation", IEEE Journal Virtual Rehabilitation. pp. 127-132.

[4] Sha, M., Varley, R. M., Richards, J., (2009), "Overcoming the information overload problem in a multiform feedback based virtual reality system for hand motion rehabilitation", International Conference on CyberWorlds., pp 51–56.

[5] Leonardis, D., Barsotti, M., Loconsole, C., Solazzi, M., Troncossi, M., Mazzotti, C. & Frisoli, A. (2015), "An EMG-controlled robotic hand exoskeleton for bilateral rehabilitation", Vol.8, No.2, pp.140 – 151.

[6] Heuser, A.; Kourtev, H.; Winter, S.; Fensterheim, D.; Burdea, G.; Hentz, V.; Forducey, P., (2007), "Telerehabilitation Using the Rutgers Master II Glove Following Carpal Tunnel Release Surgery: Proof-of-Concept", Neural Systems and Rehabilitation Engineering, IEEE Transactions, Vol.15, pp. 43 – 49.

[7] Cortese, M.; Cempini, M.; de Almeida Ribeiro, P.R.; Soekadar, S.R.; Carrozza, M.C.; Vitiello, N.A.,(2015), "Mechatronic System for Robot-Mediated Hand Telerehabilitation", Mechatronics, IEEE/ASME Transactions, Vol.20, pp.1753 – 1764 .

[8] XBee ZigBee http://www.digi.com/products/xbee-rf-solutions /modules /xbee-zigbee, Access Date: 01.04.2015.

[9] 2.2 inch Flex Sensor https://www.sparkfun.com /products /10264 Access Date: 15.04.2015.

[10] 4.5 inch Flex Sensor https://www.sparkfun.com /products /8606 Access Date: 15.04.2015.

[11] Arduino Uno, https://www.arduino.cc /en /Main /ArduinoBoardUno, Access Date: 20.04.2015.
[12] Map Function, https://www.arduino.cc /en /Reference /Map, Access Date: 23.04.2015.
[13] SG 5010 servo motors, http://www.towerpro.com.tw /product /sg5010-4/, Access Date: 20.04.2015.
[14] uLCD-32PTU touch screen, http://www.4dsystems.com.au/product /uLCD _32PTU / Access Date: 01.11.2015.
[15] DS1302 RTC datasheet, http://datasheets.maximintegrated.com /en /ds /DS1302.pdf, Access Date: 01.11.2015.
[16] Wireless SD Shield, https://www.arduino.cc /en /Main /Arduino Wireless Shield, Access Date: 12.04.2015.
[17] Arduino Mega 2560, https://www.arduino.cc /en /Main /arduino Board Mega 2560, Access Date: 12.04.2015.

BIOGRAPHIES

Aytek GÜCÜYENER was born in Istanbul, Turkey in 1982. He received the B.Sc. degrees in Electronic and Computer Education from Faculty of Technical Education, Sakarya University, in 2006. 2006 to 2011, he was a lecturer at the Istanbul Aydın University. Since 2011, he has been working as an instructor at the Arel University Vocational School Electronics Technology Program. His research areas include microcontroller systems, embedded systems, communication systems and networked control systems.

Erkan KAPLANOĞLU received the bachelor's degree from Marmara University Electric Department, in 1996. He completed his M.Sc. and Ph.D. thesis at Computer-Control Department of Marmara University, Institute for Graduate Studies in Pure and Applied Sciences, in 2000 and 2006, respectively. In March 2014, Dr. Kaplanoğlu became Associate Professor at Marmara University, Mechatronics Department. He has been awarded YGGDRASIL Award (Young Guest Doctoral Researchers in Norway) in 2010. He worked as research assistant professor at Department of Mechanical Eng. Vanderbilt University Faculty of Engineering Nashville/TN, USA from 2011 to 2012. His research areas are Biomechatronics systems, Lower limb Prosthesis, modeling, identification and control. Multivariable, Model Predictive Control, Data Acquisition Systems (DAQ).

Transient Analysis of Double Layer Metal-Gas-Dielectric-Metal DBD Cell

G.T. Alisoy. F. Hansu, B.B. Alagöz, and H.Z. Alisoy

***Abstract*— The investigation of Dielectric Barrier Discharges (DBD) in the absence of breakdown has significance in the perspective of the technological processes based on discharge phenomena and high voltage techniques. This study carries out transient analyses for the temporal evolution of electrical field, space charge density, polarization current while charging experimental Metal-Gas-Dielectric-Metal (MGDM) DBD cell. For these proposes, a theoretical model based on current continuity and two-layer polarization mechanism is developed for the investigation of an experimental MGDM electrodes system. In the steady state, the model obeys energy conservation law. Analysis results are discussed on the basis of experimental current measurements to explain pulsed DBD current.**

Index Terms— **Dielectric Barrier Discharge (DBD), MGDM system, Townsend Mechanism.**

INTRODUCTION

IN RECENT years, much attention has been paid to non-thermal plasma due to its widespread use in many fields, such as, surface modifications, lamps, plasma displays, lasers, ozone generation, environment protection, biomedical applications and particle sources [1]. According to the driving frequency of power supply, non-thermal plasma can be generated by direct current (DC), alternating current (AC), radio frequency (RF) and microwave (MW) discharges [2]. Contrary to discharges caused from RF and MW, the electrode system is an important part in DC and AC discharges because the different shapes, materials and arrangements of electrodes have an effect on gas discharges [3-7].

The DBD is commonly used in surface treatment. Therefore, DBD increases local densities of charged particles near the surface, this result in increase of surface energy and adhesion phenomena. Particularly, low-temperature gas discharge (corona, partial, glow, DBD) in electronegative gas media has been widely utilized in the modification of adhesion properties of dielectric polymers [8]. Incorporation of polar surface groups increases the surface energy and enable to cleaning or surface roughening. Furthermore, cross-linking and the formation of double bonds by chemically non-reactive species lead to surface stabilization [9]. In general, the increase in the surface energy of dielectric materials placed in electronegative gas media is explained by two mechanisms: (i) Chemical activation of the surface (the formation of free radicals on the surface) [10]. (ii) Free electrons, which are detached from negative ions, diffuse to the dielectric surface from the gas discharge region. These electrons are captured in the trap energy levels of the structure of dielectric material and as a result the electrets state form occurs [11, 12, 13]. In the MGDM electrodes systems, the charge accumulation between dielectric layers causes transient absorption and polarization currents. Measurements of these current and analysis of current characteristics have significance for the evaluation of high-voltage insulators [14]. Recently, nano-material fabrication technology benefits from dielectric barrier discharge plasma generators [15].

Another promising application of DBD is the plasma actuators developed for aerodynamic flow control [16, 17]. There are research efforts for possible use of plasma actuators in aerospace [18] and acoustic application [19]. These application uses asymmetric electrode placement to control ionic winds. Calculation of energy consumed by DBD system is an important parameter for application point of view, because the power of the system is strongly depended on the energy consumed in DBD processes. Removal of surface charge can improve flow controllability of DBD plasma actuator. Hence, electrical conduction mechanisms and charging kinetics of the DBD system are important for development of DBD applications. Honga et al. suggest an experimental method to measure surface charging of plasma actuators [20]. Several numerical simulation methods were proposed for simulation of DBD [21, 22, 23] and ionic flows [24]. However, a straight forward analytical modeling involving electro-physical mechanisms of DBD system is needed for analysis of electrical characteristic of DBD cells.

This study presents transient analyses for theoretical investigation of evolution of electrical field, free and relative charge density, current and energy-balance states for MGDM

G.T. ALİSOY, Namık Kemal University, Department of Mathematics, Tekirdag, Turkey (e-mail: galisoy@nku.edu.tr)

F. HANSU, is with the Siirt University, Department of Electrical- Electronics, Malatya, Turkey (e-mail: f_hansu@siirt.edu.tr)

B.B. ALAGÖZ, is with the Inonu University, Department of Electrical-Electronics, Malatya, Turkey (e-mail: baykant.alagoz@inonu.edu.tr)

H.Z. ALİSOY, is with Namık Kemal University, Department of Electronics and Telecomunication, Tekirdag, Turkey (e-mail: halisoy@nku.edu.tr).

Manuscript received August 09, 2016; accepted October 21, 2016.
DOI: 10.17694/bajece.292656

DBD cell models. The developed theoretical model is based on the conductivity and polarization mechanism occurred in the gap of MGDM DBD electrodes system. Experimental measurements are conducted for symmetric and circular geometry of MGDM electrodes systems composed of polyimide dielectric barrier in the gas gap. The experimental results are interpreted on the basis of analytical modeling for the case that gap voltage is lower than breakdown voltage, $|U_g| < U_{br}$, in the absence of a breakdown. In this case it can be said that diffusion and polarization mechanisms are effective in conduction of dielectric barriers. The roles of these mechanisms in Pulsed DBD currents are also discussed.

Theoretical analysis addresses the following substantial issues in order to explain charging kinetics of DBD cells made of symmetric MGDM electrodes system:

(i) Transient analysis of electrical field evolution between the dielectric layers of DBD.

(ii) Investigation of free and relative space charges between surfaces of dielectric layers.

(iii) Transient current analysis in DBD cells.

(iv) Determination of energy consumed on MGDM systems and validation of the energy balance in DBD system.

METHODOLOGY

A. Experimental Study for Metal-Gas-Dielectric-Metal DBD System

Fig. 1(a) depicts MGDM electrodes while DBD is taking place. The schematic diagram of symmetric and circular geometry of MGDM electrodes system is illustrated in Fig. 1(b). The electrical schema of experimental setup is shown in Fig. 2. This experimental setup includes adjustable low-voltage power supply, electrical noise filter, high-voltage transformer, discharge chamber and measurement apparatus. The low-voltage system consists of a coupled transformer, filter and adjustable power supply. It provides an AC voltage adjustable in the range from 0 V to 220 V. The high-voltage transformer (TR3) generates an AC voltage in the range from 0 V to 33 kV. Discharge chamber includes electrodes system and safety cover. The electrodes system is composed of two electrodes and a polyimide dielectric barrier layer in an air gap.

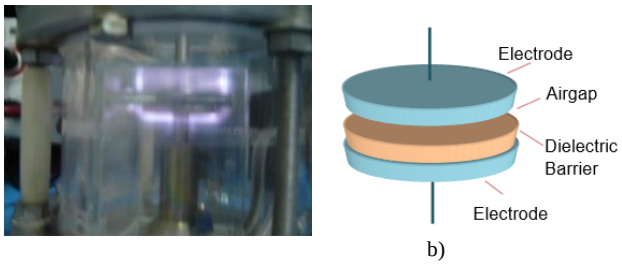

Fig.1. (a) Pictures of DBD taken place in the MGDM electrodes system (b) Schematic diagram of MGDM electrodes.

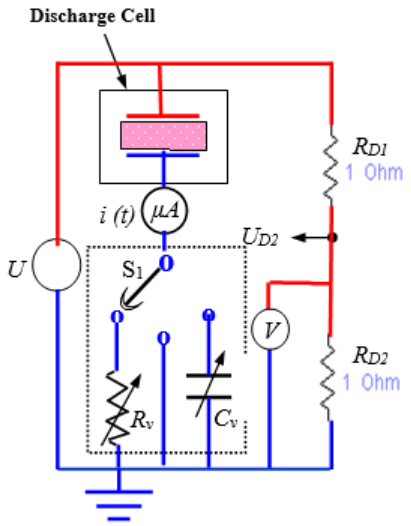

Fig.2. The experimental setup of DBD system

The DBD takes place between the two parallel plane electrodes. Both the upper and the lower electrodes are in shape of a steel cylinder and their thickness is 5 mm and the diameter is 25 mm. The dielectric barrier is made of a polyimide material film with thickness of 0.5 mm. The air gap is configured to 0.5 mm wide. The experiment was conducted in a static system in air at ambient temperature. The voltage applied to the electrodes is measured by a high voltage probe (AC High Voltage probe CT6). The discharge current and transported charges are measured by placing a 50 kΩ resistor (Rv) and a 33 nF capacitor (Cv) between the bottom electrode and the ground. The light emission image is recorded by a digital camera (Sony Cyber-Shot DSC T90) which is mounted for taking the side view of the air gap discharge. Lissajous diagram is measured by digital oscilloscope (TDS1002, Tektronix).

B. Transient Analyses of Experimental Metal-Gas-Dielectric-Metal DBD Process

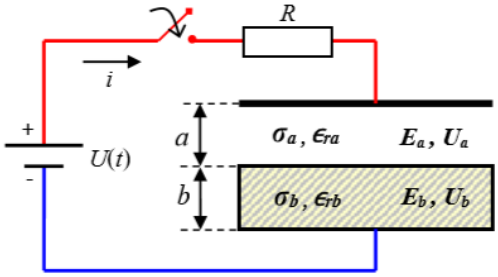

Fig. 3. Schematic diagram of the experimental MGDM electrodes system.

Figure 3 shows schematic diagram of single barrier double layer MGDM electrodes system used in DBD cell. According to Kirchoff's second law, the following equation can be written:

$$iR + U_a + U_b = iR + E_a.a + E_b.b = U \qquad (1)$$

where the parameter a is the length of gas gap, Ea is the magnitude of electrical field in the gap and Ua denotes the voltage across the gap a. The parameter b is the thickness of polyimide dielectric layer, Eb is the electrical field in polyimide layer and Ub represents the voltage drop on the polyimide layer (dielectric barrier). The voltage of MGDM system is denoted by U. The electrical current flowing MGDM system is expressed as i=JS depending on the current density J and the area of the electrode S. Considering the static electrical field, the current density is commonly written as follow:

$$J = \sigma E + \varepsilon_r \varepsilon_0 \frac{dE}{dt} \tag{2}$$

Considering current continuity condition Ja=Jb and Equation (2), the current density of MGDM system can be expressed as follow:

$$J_a = \sigma_a E_a + e_{ra} e_0 \frac{dE_a}{dt} = J_b = \sigma_b E_b + e_{rb} e_0 \frac{dE_b}{dt} \tag{3}$$

where, σ_a and σ_b are conductance of gas gap and barrier layer, ε_{ra} and ε_{rb} are the dielectric constant of layers and Ja and Jb are the current densities, respectively. By considering almost zero conductivity due to assuming air gap an ideal dielectric layer $(\sigma_a \cong 0)$ during charging in the absence of breakdown, and using the Equation (1) and (3), the following two non-homogenous equations set can be obtained for the field evolution in two layer electrode systems,

$$\begin{aligned} \frac{dE_a}{dt} &= -\frac{a}{RS\varepsilon_0 + e_{ra}} E_a - \frac{b}{RS\varepsilon_0 + e_{ra}} E_b + U \\ \frac{dE_b}{dt} &= -\frac{a}{RS\varepsilon_0 + e_{rb}} E_a - \frac{(b + RS\sigma b)}{RS\varepsilon_0 + e_{rb}} E_b + U \end{aligned} \tag{4}$$

By considering parameters of MGDM system, one can found the temporal evolution of electrical field given by Equation 5(a) and 5(b) by solving Equation (4),

$$E_a = E_{ak} + A_1 e^{p1} t + A_2 e^{p2t} \tag{5a}$$

$$E_b = E_{bk} + B_1 e^{p1} t + B_2 e^{p2t} \tag{5b}$$

In Equation (5), E_{ak} and E_{bk} parameters show steady state magnitudes of electrical fields in the layers. The parameters p1 and p2 are the Eigen values of the Equation (4). (See Appendix for the solution of the Eigen values) The parameters A1, A2, B1 and B2 are integration constants calculated depending on the initial conditions. Due to almost zero conductivity of ideal dielectric layer ($\sigma_a \cong 0$) due the condition $|U_g| < U_{br}$, the conductivity currents flowing from the gap layer of DBD cell model also becomes zero. Therefore, one can be written as the following:

$$E_{ak} . E_{bk} . b = U \tag{6}$$

Since the polyimide material film has a0 conductivity greater than zero ($\sigma_b = 10^{-10}\, S \cdot cm^{-1} > 0$), the field intensity inside polyimide barrier is taken $E_{bk} \cong 0$. In this case, the electrical field in the gas gap of our experimental DBD cell can be calculated approximately as,

$$E_{ak} \cong \frac{U}{a} = \frac{1}{0.05} = 20\ \frac{kV}{cm} \tag{7}$$

When the initial conditions are taken as $U_a(0) = U_b(0) = 0$ and considering the parameters of experimental MGDM system ($a = 500\ \mu m$, $b = 12.7\ \mu m$ and $S = 4.9\ cm^2$ in circular shape) and applied voltages ($U = 1\ kV$), the overall system current and the current densities for the experimental system is calculated as:

$$i(0) = \frac{U}{R} = \frac{10^3}{103.10^3} = 9{,}71 mA \tag{8a}$$

$$Ja(0) = Jb(0) = \frac{i(0)}{S} = \frac{9{,}71}{4{,}9} = 1{,}98\ \frac{mA}{cm^2} \tag{8b}$$

Considering these current densities, the electrical field of the experimental DBD system at $t = 0$ second can be estimated for $\varepsilon_{ra} = 1$ and $\varepsilon_{rb} = 3.56$ as,

$$\left.\frac{dE_a}{dt}\right|_{t=0} = \frac{J_a(0)}{\varepsilon_{ra}\varepsilon_0} = 22{,}372.10^9\ \frac{V}{cm.s} \tag{9a}$$

$$\left.\frac{dE_b}{dt}\right|_{t=0} = \frac{J_b(0)}{\varepsilon_{rb}\varepsilon_0} = 6{,}2845.10^9\ \frac{V}{cm.s} \tag{9b}$$

If initial conditions 9(a), 9(b) and $E_a(0) = E_b(0) = 0$ are used in Equation (5), magnitudes of electric fields in the layers of the MGDM system can be calculated as,

$$E_a(t) = 1{,}724.10^4 - 291 e^{-7{,}87.10^3 t} - 19{,}71.10^3 e^{-1135.10^3 t} \tag{10a}$$

$$E_b(t) = 5{,}5756.10^3 e^{-7{,}87.10^3 t} - 5{,}5756.10^3 e^{-1135.10^3 t} \tag{10b}$$

Under the condition of $|U_g| < U_{br}$, the relative and free charge densities collected at interface of layers can be expressed as,

$$q_s(t) = D_b(t) - D_a(t) \tag{11a}$$

$$q_s^{relative}(t) = P_a(t) - P_b(t) \quad (11b)$$

where, Da, Db, Pa and Pb parameters are the displacement flux vectors and polarization vectors of the MGDM system for the air gap and the polyimide barrier layers, respectively. These parameters can be calculated as follow:

$$D_a(t) = \varepsilon_0 \varepsilon_{ra} E_a(t) \quad (12a)$$

$$D_b(t) = \varepsilon_0 \varepsilon_{rb} E_b(t) \quad (12b)$$

$$P_a(t) = \varepsilon_0 (\varepsilon_{ra} - 1) E_a(t) \quad (12c)$$

$$P_b(t) = \varepsilon_0 (\varepsilon_{rb} - 1) E_b(t) \quad (12d)$$

The electrical field solutions given by Equation 10(a) and (b) are used in Equation 11(a) and 11(b), the characteristics of free and relative electrical charges collected between gas and polyimide layers can be expressed as follow:

$$P_s(t) = 88{,}5.(20{,}14.e^{-7{,}87.10^3 t} - 0{,}141.e^{-1135.10^3 t} - 20)\frac{pC}{cm^2} \quad (13a)$$

$$q_{sr}(t) = 1{,}26.(e^{-7{,}87.10^3 t} - .e^{-1135.10^3 t} - 20)\frac{nC}{cm^2} \quad (13b)$$

The current of MGDM system depending on the differential of electro-physical parameters of MGDM system can be obtained as:

$$i(t) = \varepsilon_{ra}\varepsilon_0 S\frac{dE_a(t)}{dt} = \sigma_b S E_b(t) + \varepsilon_{rb}\varepsilon_0 S\frac{dE_b(t)}{dt} \quad (14)$$

$$= 0,009e^{-7,87.10^3 t} + 9,7e^{-1135.10^3 t} mA$$

Besides, in MGDM systems under condition of $|U_g| < U_{br}$, by taking into account the Equations 8(a)-(b), Equations 10(a)-(b) and Equation 14, energy-balance state analyses of MGDM system can be given as:

The source energy,

$$Ws = \int_0^\infty Ui(t)dt = 10^3 \int_0^\infty (0{,}009e^{-7{,}87.10^3 t} + 9{,}7e^{-7{,}87.10^3 t})dt = 9{,}68\mu J \quad (15a)$$

The energy consumed in resistance,

$$WR = \int_0^\infty Ri^2(t)dt = 103.10^3 \int_0^\infty (0{,}009e^{-7{,}87.10^3 t} + 9{,}7e^{-7{,}87.10^3 t})^2 dt = 4{,}807\mu J \quad (15b)$$

The energy consumed in ideal dielectric (air gap) layer,

$$W_G = E_{ak}, D_{ak}.S.\frac{a}{2} = \varepsilon_{ra}\varepsilon_0 E_{ak}^2.S.\frac{a}{2} = 4{,}336\mu J \quad (15c)$$

The energy consumed in dielectric (polyimide) barrier layer,

$$W_D = \int_0^\infty \sigma E_b^2(t).S.b.dt \quad (15d)$$

$$= \sigma bS\int_0^\infty (5,5756.10^3 e^{-7,87.10^3 t} - 5,5756.10^3 e^{-1135.10^3 t})^2 dt = 0,536\mu J$$

The energy state analyses given by equations 15(a)-(d) demonstrate that the energy-balance equation WS=WR+WG+WD is valid and the energy is conserved in the experimental system. In other words, the energy delivered from the source is equal to the energy consumed in the MGDM system. This result validates the consistency of our analyses.

RESULTS AND DISCUSSIONS

In the previous section, an analytical model of experimental MGDM system was derived for the transient analyses based on the electro-physical processes in absence of breakdowns ($|U_g| < U_{br}$).

Fig. 4 shows characteristics obtained from these analyses: Fig. 4(a) illustrates the evolution of electrical fields in the gap (E_a) and in the dielectric barrier (polyimide) layer (E_a) according to Eq. 10(a) and 10(b), when 1 kV DC voltage is applied at $t = 0$ second. Electrical field reaches saturation at about 17 kV/cm in the gap and about 8 10-3 kV/cm in the dielectric barrier at. Such a high electrical field discontinuity between layers indicates an electrical charge accumulation at the interface between layers. The increase in the amount of free electrical charges as shown in Fig.4(b) confirms this charge collection phenomenon between layers. Increase of charge density on the surface of the dielectric barrier results in decrease of electrical field intensity from 5 kV/cm to 8 10-3 kV/cm. Fig.4(c) shows relative charge accumulation calculated according to the polarization vector discontinuity. Figure 4(d) shows the transient current characteristics calculated by Eq. (14). During the charge collection in the MGDM system, a sharp current pulse is drawn from the DC source. After the electrical fields in the layers reach the saturation level in 0.6 millisecond, the transient polarization currents decrease to levels of leakage currents. Therefore, the charge collection between layers slows down. In the preceding of charge accumulation on the surface of dielectric barrier, the magnitude of leakage currents is very small compared to transient polarization current. The leakage current is mainly caused from increase in the surface conductivity of the dielectric barrier depending on the surface charging of polyimide. The volume conductivity is practically ignorable compared to charged surface conductivity of polyimide due to deficiency of free charge inside the polyimide volume.

Surface connectivity and the corresponding leakage currents sharply increase as the surface charging polyimide barrier increases. Nonlinear surface connectivity mechanism behaves as if a switch controlled by the charge density and results in periodic charge and discharge current pulses.

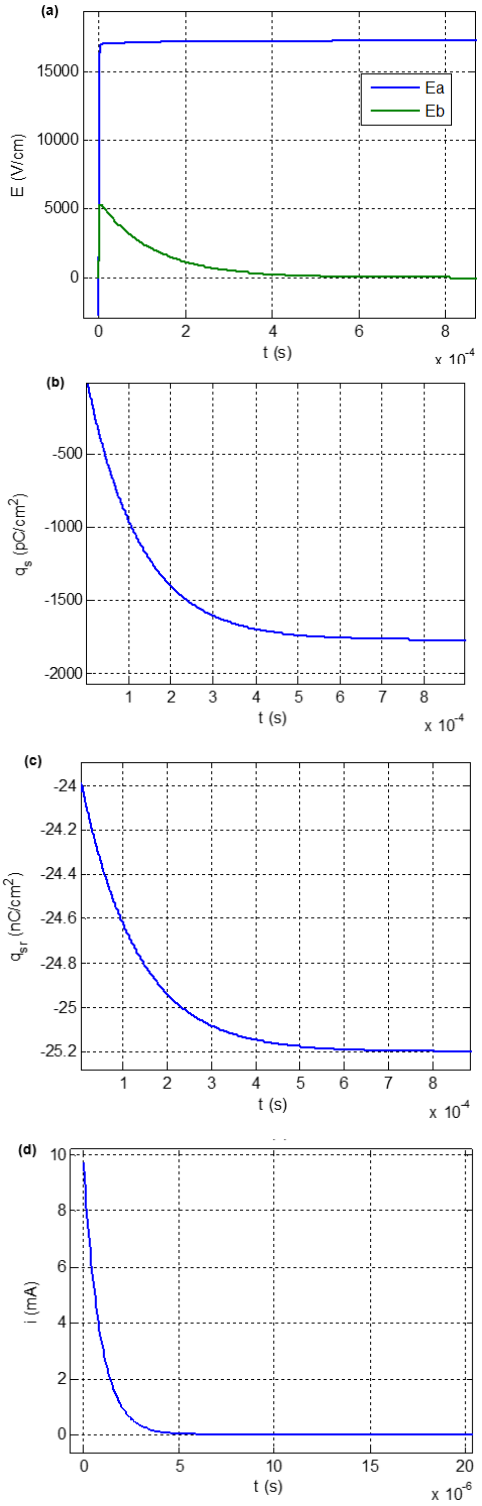

Fig. 4. Temporal evolution of electrical field intensities in layers (a), relative and free charge densities in (b) and (c), and the transient current in (d)

Fig.5(a) and 5 (b) compare measured currents from experimental setup and calculated transient current by using Equation (14). In Fig. 5 (b), transient periodical current was obtained by using the formula $i_p(t) = i(t) + i(t + n\Delta T)$, where parameter ΔT is the pulse period and $n = 1,2,3...$ The pulse period can determined from experimental measurements. Calculated current array in Fig. 5(b) presents the consistency with the measured current pulse pattern in Figure 5 (a).

When equation (14) is considered, one observes two time constant parameters; $\tau_1 = 1/p_1 = 1.27\,10^{-4}$ second and $\tau_2 = 1/p_2 = 8.8110^{-7}$ second. The τ_2 refers to the fast polarization of the air gap and the τ_1 refers to the slower polarization of dielectric barrier as seen in Figure 4 (a). Polarization of dielectric barrier is mainly results from the ions precipitation on the dielectric surface from the air gap so that, at these field intensity levels, the dielectric barrier cannot generate free charges as much as the air gap.

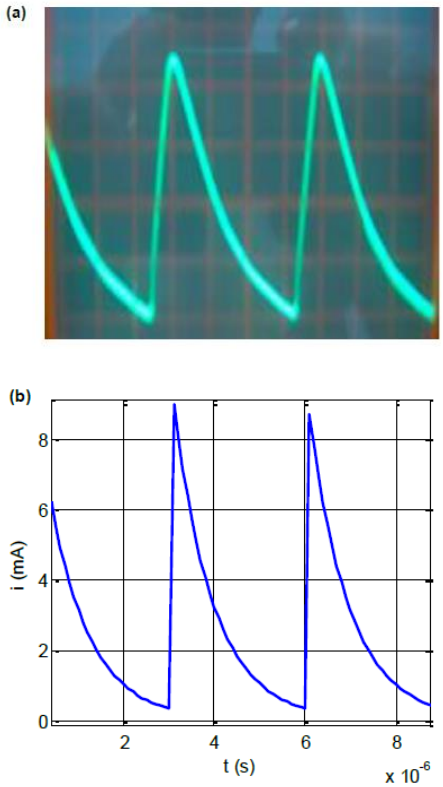

Fig. 5.(a) Experimental current of MGDM system (b) Calculated current pulse array.

Enough high electric field intensity in the narrow air gap can produce free ions due to ionization of gas molecules. These ions are accelerated by the electrical field and precipitates on the surfaces of dielectric barriers. The ions precipitations from gap result in the charging of dielectric barrier surfaces as represented in Figure 6 (a). The velocity of ionic flows determines effective depth of charge layer in the barrier surfaces. The surface charging also changes the activation energy of dielectric surface and this property is particularly useful for surface treatment applications. On the other hands, surface charging increases the surface conductivity of dielectric barriers and sharply increases leakage currents from the surfaces to the electrodes. These surface currents discharge the MGDM system and prepare it for the next charge-discharge session. This process repeats itself and results in periodic current pulses that are also known

as the Pulsed DBD (P-DBD) currents as shown in Figure 5 (a).

Subsequent charging-discharging processes of DBD are summarized by representation of the ion precipitation process in Figure 6. When the charge collection on the barrier surface reaches an adequate level, it stops further ion precipitation towards to the barrier surfaces for a while due to Coulomb force repelling free ions as in Figure 6 (b). Accordingly, a charge shield formed by Coulomb force appears near to the surface of dielectric barriers. The surface conductivity of the barriers sharply increases when charge accumulation reaches an adequate charge density on the surface. The resultant surface currents discharge the surface charges of the barrier and therefore it decreases Coulomb force to a level that initiates precipitation of the most recent charge layer as illustrated in Figure 6 (c). It increases again the surface charging of the barriers and delays ion precipitation, again. This process repeats itself and results in P-DBD currents corresponding to surface charge density of the barriers. Fundamentally, charge accumulation on the dielectric surface and the dependence of surface connectivity on charge density of the surface lead to appearing pulse trains on the measurement electrode of MGDM system.

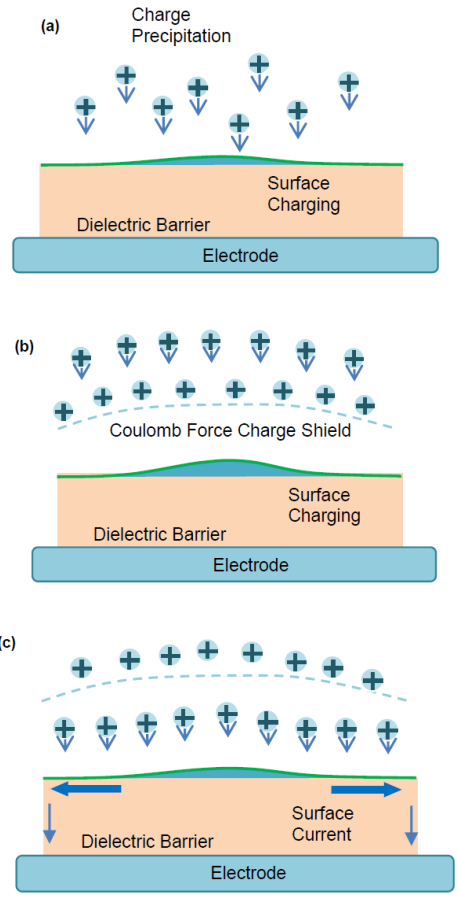

Fig. 6. A representation of charge layers on the surface.

Figure 7 shows Lissajous diagram of experimental MGDM system that shows Coulomb-Volt characteristic.

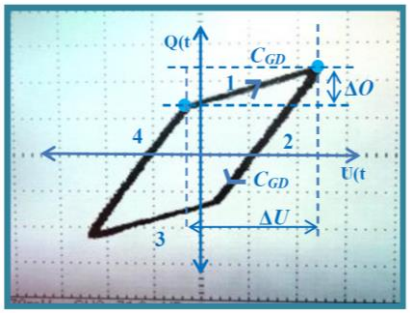

Fig. 7. Lissajous diagram of experimental MGDM system (measured by digital oscilloscope TDS1002, Tektronix)

This characteristic illustrates charging and discharging of the system for two opposite polarity of supply voltages. The figure indicates four capacitive region labeled by {1,2,3,4} according to the slope of curvatures. The charging capacitance (C_{GD1}) of MGDM system for positive voltage polarity can be calculated by the slope of line segment 1 as [25],

$$\Delta Q = C_{GD1}\Delta U \tag{16}$$

where, C_{GD1} is the charging total capacitance of MGDM system expressed as $C_{GD} = (C_D + C_G)$. ΔQ is measured from $C_v = 33\,nF$ measurement capacitance. (Vertical axis scaling is 71 mV and horizontal axis scaling is 408 V for oscilloscope screen in Figure 7) The experimental value of C_{GD1} is calculated from Lissajous diagram as,

$$C_{GD1} = \Delta Q / \Delta U = 2.3\,10^{-9} / 1019 = 2.3\,pF \tag{17}$$

Considering the increase of free charge density in Figure 4(d), one finds the deviation in charge density as $\Delta q_s = 1.76$ nC/cm2 while charging under the DC polarity voltage. Unit surface capacity of MGDM system can be obtained as,

$$c_{GD1} = \Delta q_s / \Delta U = 1.7610^{-9} / 1000 = 1.76\,pF / cm^2$$

Since, the area of the barrier layer is S=4,9cm2, the total capacity of MGDM system can be estimated as CGD=ScGD1=8,62pF. The theoretical total capacity is obtained at the level experimental value of CGD1, which is found 2.3 pF. This result shows that the analytical charging model is consistent with the experimental charging process of MGDM system for the operation region indicated the line segment 1 in the Coulomb-Volt characteristic. This confirms the relevance of theoretical calculations.

The slope of the line segment 2 yields the capacitance of MGDM system during discharge process when polarity of voltage is altered. The slope of the line segment 3 and 4 are corresponding charge and discharge capacitances for the opposite voltage polarities.

CONCLUSION

A transient analysis of experimental MGDM electrodes systems was carried for the investigation of DBD phenomenon. The purposed analytical model, based on multilayer polarization mechanisms taking place inside MGDM system, conforms to the current continuity and energy conservation laws. The calculated current waveforms are in consistency with experimental transient current measurements. The energy delivered from the source was found equal to the energy consumed in the MGDM system. The energy balance state of analytical solution confirms consistency of the model.

The analyses and experiment results are useful for explaining physical mechanism involving in DBD phenomena. In the case of multilayer systems such as MGDM electrodes systems, charge collection between dielectric layers causes polarization of the system and lead to transient polarization current. However, increasing conductivity of dielectric barrier depending on surface charging leads to periodically polarization of system and therefore it results in P-DBD currents.

In practice, the measurement of these current and analysis of current characteristics provides useful information on the electrical properties of insulation systems. Alteration in properties of insulation system can be monitored by P-DBD current measurements. In order to enhance aerodynamic flow control performance of plasma actuators, surface charge removal from dielectric barrier may be needed. Because, Coulomb force charge shielding due high surface charge density may deteriorates controlling flow direction of ionic winds. It may be helpful to use barrier material that becomes conductive when surface charge density increases.

APPENDIX

Equation (4) can be rearranged in the vector format as follows,

$$\begin{bmatrix} \frac{dE_a}{dt} \\ \frac{dE_b}{dt} \end{bmatrix} = \begin{bmatrix} k_{11} & k_{12} \\ k_{21} & k_{22} \end{bmatrix} \begin{bmatrix} E_a \\ E_b \end{bmatrix} + \begin{bmatrix} 1 \\ 1 \end{bmatrix} U \qquad \text{(A1)}$$

where,

$$k_{11} = -\frac{a}{RS\varepsilon_0\varepsilon_{ra}},\ k_{12} = -\frac{b}{RS\varepsilon_0\varepsilon_{ra}},\ k_{21} = -\frac{a}{RS\varepsilon_0\varepsilon_{rb}},\ k_{22} = -\frac{(b+RS\sigma_b)}{RS\varepsilon_0\varepsilon_{rb}}$$

Characteristic equation of the differential equation system can be written as,

$$det\begin{bmatrix} k_{11}-p & k_{12} \\ k_{21} & k_{22}-p \end{bmatrix} = 0 \qquad \text{(A2)}$$

Then, one obtains following equation, $p^2 - (k_{11}+k_{22})p + k_{11}k_{22} - k_{12}k_{21} = 0$. By solving this equation, the Eigen values of Equation (A1) can be obtained as,

$$p_1 = \frac{(k_{11}+k_{22})}{2} + \sqrt{\frac{(k_{11}+k_{22})^2}{4} - (k_{11}k_{22} - k_{12}k_{21})},$$

$$p_1 = \frac{(k_{11}+k_{22})}{2} - \sqrt{\frac{(k_{11}+k_{22})^2}{4} - (k_{11}k_{22} - k_{12}k_{21})}.$$

REFERENCES

[1] Bogaerts A., Neyts E., Gijbels R., Vander Mullen J. Gas discharge plasmas and their applications, Spectrochimica Acta Part B: Atomic Spect. Vol.57, pp.609-658 (2002).

[2] Napartovich A.P. Overview of atmospheric pressure discharges producing non-thermal plasma, Plasmas Polym. Vol.6, pp.1-14, (2001).

[3] Takaki K., Shimizu M., Mukaigawa S., Fujiwara T. Effect of electrode shape in dielectric barrier discharge plasma reactor for NOx removal, IEEE Trans. Plasma Sci. Vol.32 pp.32-38, (2004).

[4] Hepburn D.M., Kemp I.J., Richardson R.T., Shields A.J. Role of electrode material in partial discharge chemistry, Proceedings of the IEEE Fifth International Conference on Conduction and Breakdown in Solid Dielectrics, July 10–13 pp.605-610 (1995).

[5] Bhowmik S., Jana P., Chaki T.K., Ray S. Surface modification of PP under different electrodes of DC glow discharge and its physicochemical characteristics, Surf. Coat Technol. Vol.185 pp.81-91(2004).

[6] Dilecce G., Ambrico P.F., De Benedictis S. N2 density measurement in a dielectric barrier discharge in N2 and N2 with small O2 admixtures, Plasma Sources Sci. Technol. Vol.165, pp.11–522 (2007).

[7] Golubovskii Y.B., Maiorov V.A., Li P., Lindmayer M. Effect of the barrier material in a Townsend barrier discharge in nitrogen at atmospheric pressure, Journal of Phys. D: Appl. Phys. Vol.39, pp.1574-1583 (2006).

[8] Alisoy H.Z., Baysar A., Alisoy G.T. Physico-mathematical analysis of surface modification of polymers by glow discharge in SF6+N2 medium, Physica A: Statistical Mechanics and its Appl. Vol.351 pp.347–357 (2005).

[9] Massines F., Gouda G., A comparison of polypropylene-surface treatment by filamentary, homogeneous and glow discharges in helium at atmospheric pressure, Journal of Physics D: Applied Phys. 313, pp.411-3420 (1998).

[10] Amirov I.I., Izyumov M.O. Reactive ion etching of polymer films in an oxygen inductively coupled radiofrequency-discharge plasma, High Energy Chem. Vol.33,pp.119-123 (1999).

[11] Juvarly C.M., Aliyev (Alisoy) H.Z., Gorin Yu.V., Leonov P.V. On the role of the negative ions in the modification of the surface by electrical discharge, J. Surface Engineering and Applied Electrochem. Vol.138 pp.39-41 (1987).

[12] Juvarly C.M., Gorin Yu.V., Leonov P.V., Aliyev (Alisoy), H.Z. Process, Destruction and Stabilization of Polymer Materials, Proceedings of the Symposium on, IFRON, Dushanbe, 226 (1983).

[13] G.M. Sessler, Ed., Electrets, Berlin, Heidelberg, New York, (1980).

[14] Razevig D.V. High voltage engineering, Khanna Publishers, (1972).

[15] Bednara N., Matovićb J., Stojanovića G. Properties of surface dielectric barrier discharge plasma generator for fabrication of nano materials, J. Electrostat. Vol71 pp.1068–1075(2013).

[16] Kriegseis J., Möller B., Grundmann S., Tropea C., Capacitance and power consumption quantification of dielectric barrier discharge (DBD) plasma actuators, Capacitance and power consumption quantification of dielectric barrier discharge (DBD) plasma actuators, J. Electrostat. Vol. 69, pp.302–312 (2011).

[17] Roth J.R. Aerodynamic flow acceleration using paraelectric and peristaltic electrohydrodynamic effects of a one atmosphere uniform glow discharge plasma, Physics of Plasmas, Vol.10 pp.1166–1172 (2003).

[18] Shang J.S., Surzhikov S.T., Kimmel R., Gaitonde D., Menart J., Hayes J. Mechanisms of plasma actuators for hypersonic flow control, Progress in Aerospace Sci. Vol.41 pp.642–668 (2005).

[19] Li Y., Zhang X., Huang X. The Use of Plasma Actuators for Bluff Body Broadband Noise Control, Experiments in Fluids, Vol.49, pp.367–377 (2010).

[20] Honga D., Rabata H., Pub Y.K., Leroyc A. Measurement of the surface charging of a plasma actuator using surface DBD, Journal of Electrost. Vol.71 pp.547–550 (2013).
[21] Shkurenkov I.A., Mankelevich Y.A., Rakhimova T.V. Two-dimensional simulation of an atmospheric-pressure RF DBD in a H2 : O2 mixture: discharge structures and plasma chemistry, Plasma Sources Sci. Technol. 22 (2013) 015021.
[22] Hoskinson A.R., Hershkowitz N. Double DBD Plasma Actuator Simulations and Experiments in Quiescent Air, Plasma Science, IEEE 34th International Conference on, (2007).
[23] Flores-Fuentes A.A., Peña-Eguiluz R., López-Callejas R., Mercado-Cabrera A., Valencia A. R., Barocio S.R., Godoy-Cabrera O.G., Piedad-Beneitez A. de la, Benítez-Read J.S., Pacheco-Sotelo J.O., Modelling and simulation of a DBD plasma discharge supplied by a multicell inverter, In Proceedings of the 25th IASTED international conference on Modeling, identification, and control (MIC'06), M. H. Hamza (Ed.). ACTA Press, Anaheim, CA, USA, pp.249-254 (2006).
[24] Alisoy H.Z., Alagoz S., Alisoy G.T., Alagoz B.B., An Investigation of Ionic Flows in a Sphere-Plate Electrode Gap, Plasma Sci. Technol. Vol.15: pp.1012-1019 (2013).
[25] Kuchinskii G.S., Partial Discharge in High Voltage Constructions, L. Energy, 1979.

BIOGRAPHIES

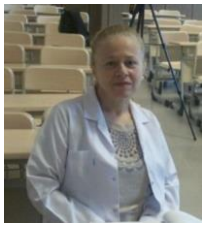

GULIZAR ALISOY, was graduated with honors from the Faculty of Mathematics and Mechanics of the Azerbaijan State University. Her M.Sc.(85') and Ph.D. (97').She received Assoc. Prof. degree in Analysis and Theory of functions from High Education Council of Turkey in 2012. Currently, she is Assoc.Professor, in Mathematical Department of Namik Kemal University. Her research interests are, integral representation of multi-package variable functions, differential properties of functions, mathematical modeling of engineering problems.

FEVZI HANSU, was graduated from University of Inonu, department of Electrical and Electronics Engineering in 2001. He worked for Kalyon Plastic and Man-Olp for several years. He is following Ph.D. at Inonu University department of Department of Electrical-Electronics Engineering. He has been working as an Asst. Prof. at the Siirt University, Department of Electrical and Electronics Engineering.

BARIS BAYKANT ALAGOZ, was graduated from University of Istanbul Technical University department of Electronics and Communication Engineering in 1998. He worked for Alcatel Microelectronics and Turkish Telecom for several years. He is following Ph.D. at Inonu University department of Department of Electrical-Electronics Engineering. He has been working as an Asst. Prof. at the Inonu University, Department of Electrical and Electronics Engineering.

HAFIZ Z. ALİSOY, was graduated from Moscow Technical University department of ElectroPhysics Engineering 1982. He had his PhD degree from USSR Science Academy Physics Institute of P.N. Lebedyev and Doctor of Sciences degree (DSc) from International Ecology-Energy Academy. He became as Full Professor in 1995. He received award of Young Scientist. He works at Namık Kemal University, Department of Electronics and Telecommunication Engineering.

Statistical Analysis of Partial Discharges

E.Onal, U. Aktepe and Y. Baygar

***Abstract*— In this paper, a statistical analysis method is applied to partial discharge (PD) measurements for the quality assessment of electrical insulation in high-voltage equipment. The rod plane electrode system in magnetic field and non-magnetic field is selected as test environment. This data helps to showing scattering and concentration of values. In this study, the partial discharge values of electrode system under magnetic field is higher and more scattering than that of electrode system under non-magnetic field. Moreover, Box and Whisker method used in this study gives a lot of information compared other statistical methods.**

Index Terms—**Partial Discharges, Box-Whisker Plot, Magnetic Field, High Voltage.**

I. Introduction

EFFICIENT generation, transmission and distribution of electricity is one of the important issues of electrical engineering. The stability of the electrical system is related to the state of high voltage components used in system. Problems that may arise in high voltage components can affect the stability of the system and this will lead system not to get desired efficiency. One of the events that can cause problems for the components of system is electrical discharges. The electrical discharges which is the state in which the insulating material becomes electrically conductive are studied in two groups (complete and partial discharges). Partial discharge is electrical discharge which does not fully bridge the insulation. Partial discharge is called as a localized dielectric breakdown. Although partial discharges are usually small in size, they can cause growth problems and can cause the material to deteriorate. Partial discharge is a generic term for discharge events that are not completely realized. The concept of partial discharge includes different groups. These groups can be examined in internal discharges, surface discharges, corona discharges and electrical treeing [1-4]. A lot of study has been done from the past on the subject of partial discharge. Although there are many studies on partial discharge concept, there are few studies on the effect of the magnetic field [5-9]. In this study the effects of the magnetic field on the partial discharge signals are investigated statistically.

E. ONAL, Istanbul Technical University, Department of Electrical Engineering, Istanbul, Turkey. (e-mail: eonal@itu.edu.tr)

U. AKTEPE, Istanbul Technical University, Department of Electrical Engineering, Istanbul, Turkey. (e-mail: aktepeu@itu.edu.tr)

Y. BAYGAR, Istanbul Technical University, Department of Electrical Engineering, Istanbul, Turkey. (e-mail: yaseminzeybekoglu@yahoo.com)

Manuscript received September 19, 2016; accepted December 26, 2016.
DOI: 10.17694/bajece.292659

II. Experimental and Statistical Research About Partial Discharge

0.220/100 kV test transformer, coupling capacitance having the value of 1nF, measuring impedance and measuring device are used at experiments. Firstly, the rod-plane electrode system is selected to form and the test setup is established. Electrode gap spacing is selected as 35 mm. By selecting this electrode gap spacing, partial discharge analysis can be performed more safely without breakdown. The rod electrode used in the experiments is 67 mm long, 2 mm thick and chrome plated. In addition, the radius of the tip of the rod electrode is 1 mm. The plane electrode is 10 mm thick, 75 mm in diameter and has a radius of curvature of 3 mm.

Secondly, the high voltage test system to be applied to the selected electrode system is set in two different ways. A high voltage test transformer, a resistor and a capacitive voltage divider are used to apply high alternating voltage to the electrode system. On the plane electrode, plexiglass box with adjustable range is placed. The plexiglass box used for the magnetic field setup is also used in this setup to be identical. Plexiglass box thickness is 3 mm. The distance between the two outer surfaces of the plexiglass to be used in the experiment is selected as 10 mm. The electrical measurement is carried out by means of a partial discharge measuring device (Haefely DDX-9121) and a computer via a coupling capacitor connected in parallel with the high alternating voltage generation test system. Two neodymium cylindrical magnets are added to the system after the partial discharge inception voltage obtained in the absence of the magnetic field. Cylindrical magnets are added to the plexiglass box to create a changing magnetic field. In the analysis part, the data obtained from the tests performed are examined. At this case magnetic field is approximately 100 mT. Firstly, the effects of the magnetic field on the partial discharge inception voltage are investigated. Data obtained in the case of no magnetic field for different vertical and horizontal openings and data obtained in the presence of magnetic field using cylindrical magnets are compared in terms of partial discharge inception voltage in graphs. In this study, the gap of plexiglass box is selected as 10 mm. At here, the first aim is to find the effect of magnetic field on partial discharge and secondly to examine the data statistically as using box and whisker method. When the obtained graphs are examined, it is found that the presence of the magnetic field lowers the value of the partial discharge inception voltage. Since the magnetic flux density is greatest when the distance between the magnets is the smallest, the greatest effect is seen in the horizontal opening of 10 mm. As the distance between the magnets increases, the magnetic flux density decreases, so the effect on the partial discharge

starting voltage also decreases. The percentage reduction in the partial discharge inception voltage values is also determined by changing the magnetic flux density values. The largest decrease in the percentage of the partial discharge inception voltage value is found to be the value at which the magnetic flux density is the greatest.

It is important to note that statistical parameters calculated from various discharge distributions can help to determine the type of discharge source and the development of its activities. Therefore the results may be useful for the improvement of PD recognition fingerprints. Thus, successful PD recognition must be based on reliably performed measurements.

In the high-voltage laboratory, an experiment is conducted under the examination of the effect of magnets on partial discharge. Two separate data sets are obtained in two different experiments. Firstly, when there is no magnetic field, partial discharge signals are produced by increasing the voltage with a variac. The discharge magnitude and voltage values of each passing time of the generated signals are recorded on a computer with a partial discharge measuring device. Secondly, this time the same experiment is carried out with the magnetic field and the data are obtained. The discharge magnitudes (pC) due to the increased voltage for two experiments are shown in Figure 1.

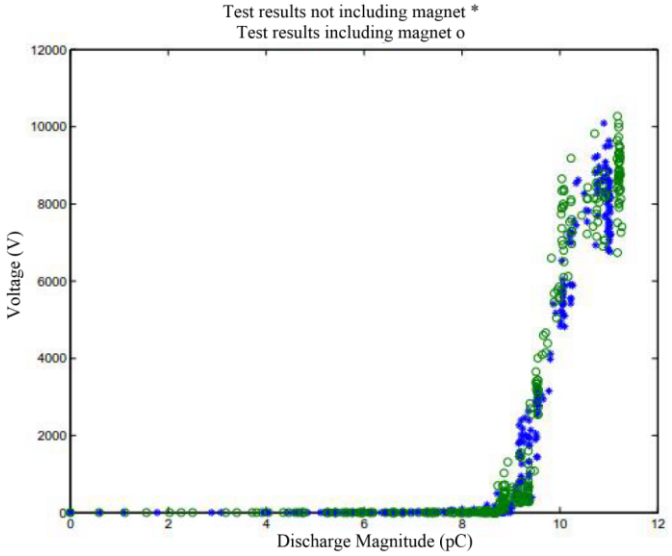

Fig. 1 Voltage-Discharge magnitude graph

Analytical methods used in partial discharge studies are generally Normal distribution, Log-normal distribution, Exponential distribution, Gamma distribution, Rayleigh distribution, Gumbel distribution and Weibull distribution. The data is gathered, organized, computed and interpreted in order to perform a statistical research or survey [10]. There are several ways of representing statistical data which include tabular representation as well as a graphical representation. In statistics, various different graphical methods are explained. For example - line plot, scatter plot, histogram, frequency polygon, ogive etc. There is one more useful graph which is known as a box and whisker plot. The Box and Whisker Method is a graph that shows the graph data according to the central distribution. In statistics, it is assumed that the data points are grouped or clustered around a value called central value. The box and whisker plot contains boxes and tails called whiskers. A box contains the highlight points, or central values i.e. the middle half of the given data points. The whisker reflects the other half of the data points. Box and Whisker Method is shown at Fig. 2 schematically.

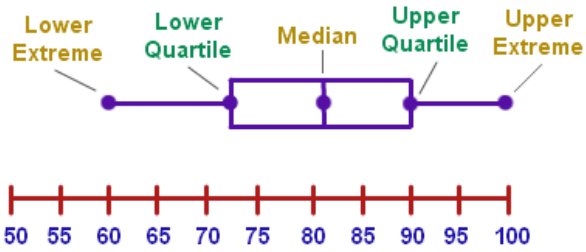

Fig. 2 Box and Whisker Plot

The following studies are conducted in terms of being suitable statistical distribution,

- The applied voltage values are grouped in 0.5 kV intervals.
- Since there is quite a small number of discharges occurring at voltages below 6 kV, these measurements are removed from the dataset.

The box and whisker plot is a very convenient way of representing groups in a numerical data. These plots help in reflecting the differences between data points which are made without assuming the underlying statistical distribution. Box and whisker plot is very useful in understanding distribution of the data and its quartiles. They summarize data from multiple sources and display the results in a single graph. Box and whisker plots allow for comparison of data from different categories for easier, more effective decision-making [11]. A Box-Whisker chart is drawn for each experiment with the new data set as Figure 3 and Figure 4.

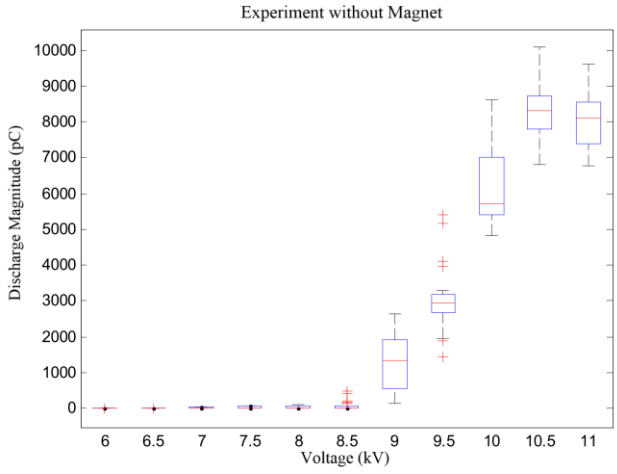

Fig. 3 Box-whisker graph for the experiment without magnet

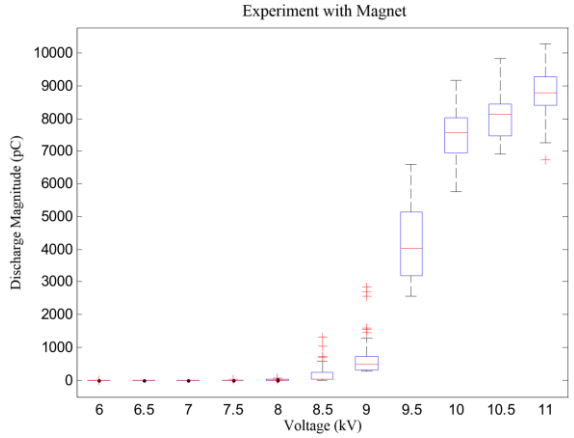

Fig. 4 Box-whisker graph for the experiment with magnet

The results of two experiments are required to be on a common scale for comparison and evaluation. Therefore,

- The experimental voltages and the discharge magnitudes of these voltages, which are rarely seen in discharges (V < 8 kV), have been removed from the data set. To cut the upper limit from a certain point, 11 kV<V voltages and the discharge amplitudes of these voltages are also subtracted from the data set.
- The measurements obtained from the voltage level after the voltage increase is stopped are removed from the data set.

By using the existing data sets, a curve of the third order is formed for the magnetic and non-magnetic states and plotted together with the actual data as in Fig.5 and Fig.6.

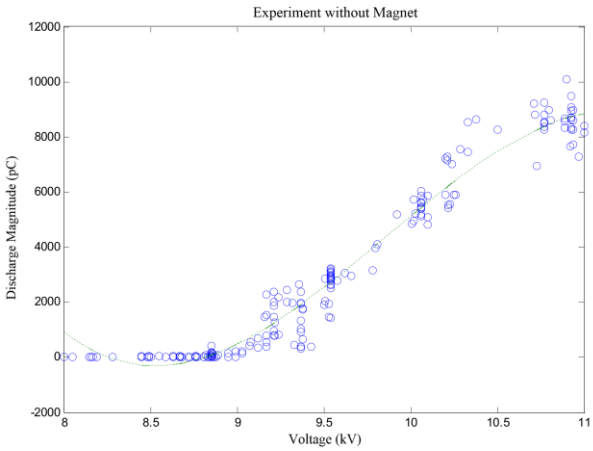

Fig. 5. Curve fitting in the experiment without magnet.

The curve fitting the two experiments is shown in Figure 7 on the same graph. It is seen that the discharge amplitudes in the case where the magnet is used are larger than the non-magnet state.

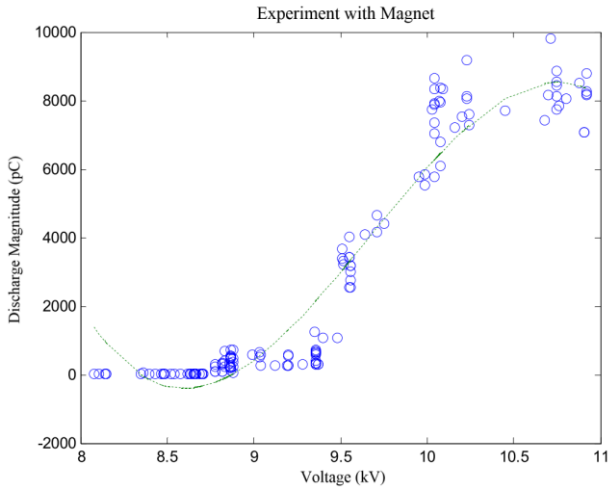

Fig. 6. Curve fitting in the experiment with magnet

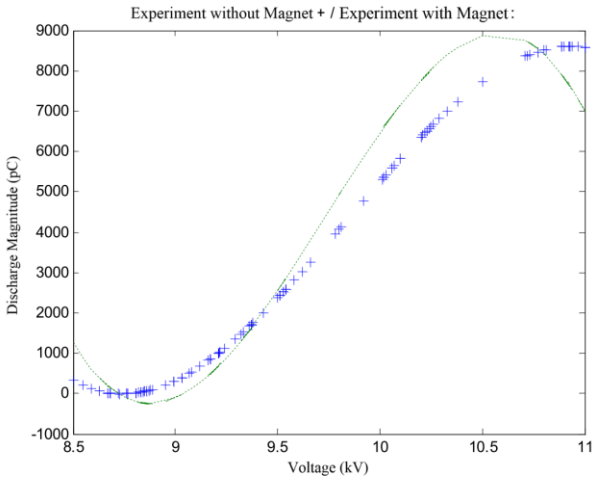

Fig.7. Curve comparison

III. CONCLUSIONS

Box plot is a graphical display that simultaneously describes several important features of a data set, such as center, spread, departure from symmetry, and identification of observations that lie unusually far from the bulk of the data. It not only consists of a rectangular box representing the inter-quartile range of the data as well as indicating the lowest and highest observations. There is a line drawn across the box at the median of the data set and whiskers that extended from each end of a box. The lower whisker is a line from the first quartile to the smallest data point within 1.5 inter-quartile ranges from the first quartile. The upper whisker is a line from the third quartile to the largest data pint within 1.5 inter-quartile ranges from the third quartile. Box plots are particularly useful in graphical comparisons among data sets, because they have high visual impact and are easy to understand. For example, figures 3 and 4 show, in each category, comparative box plots for three distribution variables. There, the statistical analysis of breakdown processes focuses basically on the estimation of the breakdown voltage. It is observed, that the breakdown-measurements have basically different dispersion than

measurements in magnetic field. In non-magnetic field we see normal like distributions with relatively low scatter, in magnetic field, the distribution is different and the scatter clearly increased. Taking into account, that the PD is a breakdown-like process, it seems likely, that the measured PD parameters have different dispersion and distribution as well. So, from the results can be derived, that the distributions of the measured PD parameters in the two setups differ significantly from each other. Therefore, box plots give a graphical summary of three distribution variables used in this investigation, which help to have a close look over the data range of selected distribution variables thus identify the accepted range as well as the extreme value.

As seen figure 5 and figure 6, scattering and amplitudes of partial discharges increased. Corona inception voltage for this two cases is approximately 9.5 kV. The effect of magnetic field on corona inception voltage could not be observed. For example, at 10.5 kV, the partial discharge with magnetics field is about % 15 higher than that of without magnetic field. This study can be expanded by adding new statistical techniques.

REFERENCES

[1] Reid, A. J., Hepburn, D. M. & Stewart, B. G. (2013). The influence of external magnetic fields on the partial discharge characteristics of voids. *Electrical Insulation Conference*, Canada.

[2] Hauschild, W. & Lemke, E. (2014). *High-Voltage Test and Measuring Techniques*, Springer, Berlin.

[3] Sipocz, T., Skalny, J. & Veis, S. (1977). The effect of the magnetic field on the positive corona discharge. Czech. J. Phys. B 27, pp. 418-421

[4] Moon, J., Lee, G. & Chung, S. (1999). SO_2 and CO gas removal and discharge characteristics of a nonthermal plasma reactor in a crossed dc magnetic field. *IEEE Transactions on Industry Applications*, vol. 35, no. 5, pp. 1198-1204.

[5] Mi, J., Xu, D., Sun, Y., Du, S. & Chen, Y. (2008). Influence of magnetic fields on negative corona discharge currents. J. Electrostatics, Vol. 66, pp. 457-462.

[6] Pekarek, S. (2010). DC corona discharge ozone production enhanced by magnetic field. European Phys. J. D, Vol. 56, pp. 91–98.

[7] *Trans. Dielectrics and Electrical Insulation*, 18(6):1813-1820.

[8] Arora, R. & Mosch, W. (2011). High Voltage and Electrical Insulation Engineering, IEEE Press, New Jersey.

[9] M. H. Hayes,M.H, Statistical Digital Signal Processing and Modelling, 1996.

[10] Bahadoorsingh S., Sambeharry S., *Electrical Treeing Diagnostics - An Approach Combining Optical Measurements and Partial Discharge Statistics*, 2006.

[11] Tarifa, J. M. M., Conde, J. R., Robles, G. & Feito, J. S. (2010). Influence of leakage magnetic fields on partial discharge activity in power transformers. *IEEE Transactions on Dielectrics and Electrical Insulation*, vol. 17, no. 6, pp. 1724-1730.

[12] Bhangaonkar, S., Kulkarni, S. V. & Shevgaonkar, R. K. (2011). Study of the effects of alternating magnetic field on point-plane corona. *IEEE.*

BIOGRAPHIES

EMEL ONAL was born in Istanbul, Turkey. She received B.Sc., M.Sc. and Ph.D. degrees from Istanbul Technical University (ITU) in Electrical and Electronics Faculty in Istanbul, Turkey. She worked as a visiting researcher at IEH Stuttgart University about GIS technology and transformers between 2006 and 2007. She is currently working as a Assoc. professor in electrical engineering department at ITU and her interest areas are in the areas of discharge phenomena, electrical power systems, insulation and protection techniques in power systems, generation and measurement of high voltages, signal processing, soft computing and condition monitoring techniques.

UGUR AKTEPE was born in Istanbul in 1990. He received the B.S. degree and the M.S. degree in electrical engineering from Istanbul Technical University, Istanbul, Turkey, in 2014 and 2016, respectively. His research interest is partial discharge measurement. He is currently doing his PhD in electrical engineering at Istanbul Technical University.

YASEMIN BAYGAR is currently working at Siemens A.Ş. as Senior Electrical Engineer. She is a Ph.D. candidate at İTÜ, Electrical Engineering Department. She also received her B.S. and M.S. degrees in Electrical Engineering from İTÜ.

The Training of Renewable Energy Systems: Undergraduate Studies

V. Esen, S. Varbak Nese, S. Saglam, B. Oral

***Abstract*— As in all over the world, interest in usage of renewable energy sources has increased in Turkey. Due to intersection of universities leadership on the research and the technology field with the renewable energies innovative feature, it is convenient to provide these provide renewable energy trainings in higher education. To provide practical training to have qualified personnel, new laboratories are required to be established in this field. Therefore, it is becoming extremely important to provide practical training in the field of renewable energy at undergraduate and postgraduate level in universities. In this study, practical working example is provided the scope of has been established in technical equipment of the renewable energy laboratory within Marmara University Faculty of Technology Electric Electronic Engineering Department. This study intends to provide guidance to further studies in renewable energy education.**

Index Terms—**Engineering education, Power engineering education, Renewable energy sources, Vocational training.**

I. Introduction

ENERGY needs of countries is increasing due to the improvement of life quality and technological development [1,2]. Besides, public awareness on the environmental impact of fossil fuels formed and environmental incentives of governments has increased the interest in renewable energy sources [3,4]. Concordantly, new energy policies of many countries are directed to the use of clean and renewable sources [1]. As a result of the growing encouragement and technological development in the field of renewable energy, requirement for more research and technical people has emerged as a growing need [5]. Engineering education plays a crucial role in meeting this need in the whole education system [6].

V. ESEN, Istanbul Arel University, Vocational School, Department of Electricity, Sefakoy Campus, Istanbul, Turkey. (e-mail: vedatesen@arel.edu.tr)

S. VARBAK NESE, Marmara University, Technology Faculty, Department of Electrical and Electronics Eng., Istanbul, Turkey. (e-mail: secil.varbak@marmara.edu.tr)

S. SAGLAM, Marmara University, Technology Faculty, Department of Electrical and Electronics Eng., Istanbul, Turkey. (e-mail: ssaglam@marmara.edu.tr).

B. ORAL, Marmara University, Technology Faculty, Department of Electrical and Electronics Eng., Istanbul, Turkey. (e-mail: boral@marmara.edu.tr)

Manuscript received October 20, 2016; accepted December 29, 2016.
DOI: 10.17694/bajece.293144

Development of theoretical and practical concepts in engineering training is based on practical experiments. [7]. In this context, undergraduate and graduate levels of renewable energy education, besides the technical information students to gain the creative and innovative features, it is possible with practical work [8].

The present study highlights the importance of supporting students with the application of theoretical knowledge in the field of renewable energy. In Marmara Universtiy Technology Faculty founded a RES (Renewable Energy Sources) laboratory for the undergraduate and graduate students to be able to conduct practical work. The technical equipment and the examples of applications in the said laboratory are presented in detail.

II. Renewable Energy Education in the World and Turkey

Education is vital in social development and energy is key to sustainable development [9, 10]. Increased sensitivity about energy security of countries, supporting policies and decreasing energy costs have increased the integration of renewable energy systems to the power system. 100 GW of renewable energy capacity has been added to power system in the last three years worldwide [11].

As is the case in all development processes, this rapid progress has created the need for qualified personnel. To meet the need, diversified training programs have emerged [10]. In the world, renewable energy education at undergraduate level includes various courses and research programs [12]. However, graduate programs have a priority compared to undergraduate program in renewable energy education [13].

Today, there are no private programs at undergraduate level in the field of renewable energy [10]. However, graduate programs on renewable energy sources are offered, and short-term training programs are also available. In addition, associate degree programs are offered in the United States and a large number of vocational courses are available in many European countries [13]. Increasing the usage of renewable energy sources in Turkey is inevitable for the following reasons [1]:

- Import dependency (more than half of its energy),
- Limited fossil energy sources,
- Rapidly growing energy consumption,
- Increased environmental awareness,
- Advantages of geographical position for the usage of renewable energy sources.

In Turkey, 4% of electricity generation was provided from renewable energy sources of the country in 2014; and the utilization of renewable energy sources for the purpose of electrical energy generation is promoted by the related laws and regulations [14].

This field has steadily increasing number of advantages and incentives and accordingly education on the field should be offered in line with the following aims [1]:

- To increase public awareness and introduce basic concepts through short-term courses at college level and media,
- To meet the need for trained field staff with certificate and diploma courses,
- To meet design, development and evaluation needs with the bachelor's degree in the field of energy engineering,
- To train scientists and engineers with graduate courses for sustainable development of technology.

However, renewable energy education in Turkey is mostly offered at the tertiary level [15]. Although graduate training has focused on renewable energy sources, elective courses are rapidly increasing in the related departments. In addition, vocational courses are offered for field staff [16].

III. LABORATORY SCOPE AND EXPERIMENTS

In the laboratory, experiments are planned to explain scientific and engineering fundamentals of renewable energy based electricity generation. Cognitive experiences of the students are supported by psychomotor experiences for persistent skills development using laboratory equipment. Wind and solar energy test equipment are used to recognize wind and solar components in the power systems. During the selection process of the test equipment, their specific qualities such as their usability for different applications and adaptability for new technologies are taken into consideration. Therefore, test equipment is convenient for graduate level trainings.

For scientific researches, the laboratory is equipped with professional solar simulator (Fig. 1). In the simulator, AM 1.5 solar spectrum intensity can be obtained from a circle of 16 cm in diameter with 300W ceramic xenon lamp. Also, ambient temperature change is only 3-4^{0}C. So, it can be used to explore solar cells and their characteristics. At the same time, age related efficiency changes and power quality effects for grid connections of photovoltaics can be examined under simulated real conditions. As a power quality study, the effects of harmonics generated by electronic inverter can be examined for grid connection.

In addition to graduate level studies, undergraduate level experiments which can be carried out in solar equipment (Fig. 2) and their supplementary benefits for technical equipment usage are listed below.

- Light intensity and temperature measurements: Different types of light source are used to measure and examine light intensity using Solarimeter, Luxmeter and Pyranometer. Photovoltaic panel surface temperature is measured with infrared thermometer.
- Exploring photovoltaic panels: Photovoltaic panel peak voltage and peak load current are measured and compared with the panel production values.
- Load effects on photovoltaic panel output voltage: Different types of loads are used to examine the effects of load characteristics on photovoltaic panel output voltage.

Fig. 1. Solar simulator

- Temperature effects on photovoltaic panel output voltage: Photovoltaic panel surface temperature is increased incrementally and photovoltaic panel output voltage is measured and analyzed.
- Inverter output voltage-Load type correlation: Under the fixed light intensity, inverter output voltage is measured and analyzed using power quality analyzer for different load characteristics (Fig. 3).

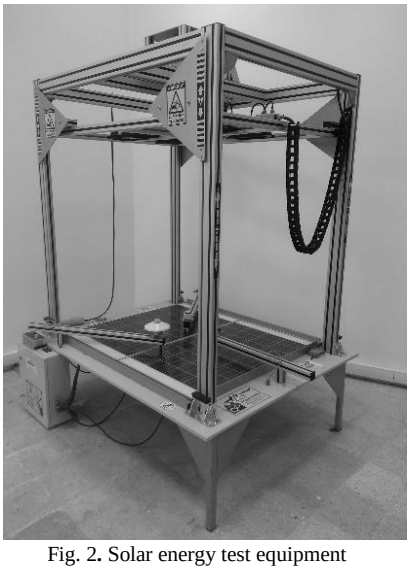

Fig. 2. Solar energy test equipment

In the wind energy test equipment, 0-12 m/s wind speed can be supplied (Fig. 4). On the other hand, the distance between fan and wind turbine can be changed to increase wind speed. Different wind turbines with suitable dimension blades and

turbine simulators can be tested. So, graduate level studies for the determination of optimum load conditions, blade design, pitch angle control, blade faults and electrical faults of generator can be realized. In addition to these studies, wind energy experiments for undergraduate level are listed below and necessities of them are explained.

Fig. 3. Data acquisition and measurement instruments

- Wind speed measurements: This parameter is very important to determine the area to install a wind turbine/farm. The measurement of wind speed is performed with this experiment to teach anemometer usage, possible measurement errors and the parameters which affect wind speed knowledge.
- Wind speed-wind turbine cycle correlation: Cut-in and cut-off speeds, tachometer usage and vibration measurement qualifications are introduced to the trainees in this education program.

Fig. 4. Wind energy test equipment.

- Wind speed-output voltage of wind turbine correlation: Wind speed value can be changed in this test-rig. So, output voltage change, wind turbine response can be analyzed according to wind speed changes.
- Wind speed-load current of wind turbine correlation: Load current changes with wind speed can be investigated. The efficiency of investigated wind turbine in terms of meeting load demand is explored.
- Exploring output power of wind turbine for different loads: Output power is explored for different load types. So, the person who completes this program gains knowledge about interconnecting of turbine response.

For measurements from test equipment a Matlab/Simulink program is generated (Fig. 5). Data of wind and solar energy test equipment rigs are transferred to computer through data acquisition card. This measurement type is preferred because of its feasibility. The students can also practice the basics of data acquisition and signal processing techniques.

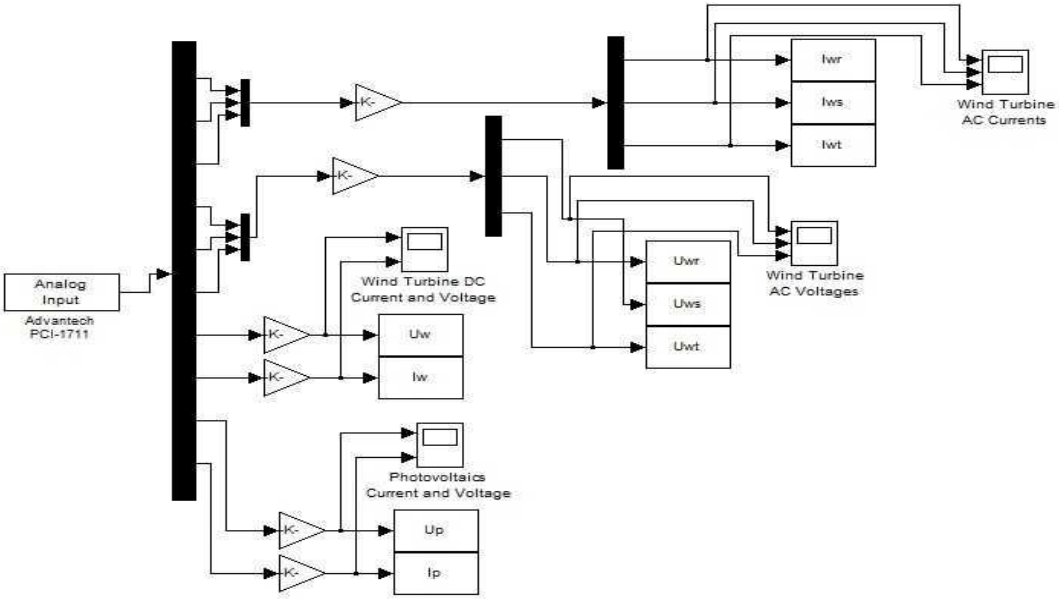

Fig. 5. Hybrid system Matlab Simulink Model

IV. CONCLUSION

All over the world, with the increased use of renewable energy sources the training of qualified personnel has become mandatory in the sector. It is possible to train qualified personnel who have the skills to follow new technologies, plan, make decisions, manage and apply projects according to local conditions. In this study, a new test equipment was designed utilizing previous studies in order to provide trainees with the basic engineering skills in this field.

In this context, the following training outcomes are identified, learned, understood and applied by the trainees.

- Renewable energy sources used for electrical energy generation,
- Principles of energy conversion,
- Measurement and evaluation of meteorological data,
- System response according to meteorological conditions,
- Determining the appropriate field conditions and installation of renewable energy conversion systems,
- Solar and wind based electrical energy generation in power systems,
- The operation of hybrid systems,
- Grid connection and power quality,
- Results of extreme operation conditions (faults, strain, etc.).

ACKNOWLEDGMENTS

This project is supported by the Marmara University Scientific Research Committee. Project No: FEN-E-120514-0149

REFERENCES

[1] C. Acikgoz, "Renewable energy education in Turkey", Renewable Energy, vol.36, pp.608-611, 2011.
[2] M. Bojic, "Education and training in renewable energy sources in Serbia and Montenegro", Renewable Energy, vol. 29, pp. 1631-1642, 2004.
[3] G. G. Alcaraz, E. Galván, N. G. Cabrera, M.S. Javadi, "Renewable energy resources short-term scheduling and dynamic network reconfiguration for sustainable energy consumption", Renewable and Sustainable Energy Reviews, vol. 52, pp. 256-264, Dec. 2015.
[4] V. Franki, A.Viskovic, "Energy security, policy and technology in South East Europe: Presenting and applying an energy security index to Croatia Energy", vol. 90, no. 1, pp. 494-507, Oct. 2015.
[5] H. Malkki, K. Alanne, L. Hirsto, "A method to quantify the integration of renewable energy and sustainability in energy degree programmes: a Finnish case study", Journal of Cleaner Production, vol. 106, pp. 239-246, 2015.
[6] E. Kacan, "Renewable energy awareness in vocational and technical education", Renewable Energy, vol. 76 (2015) pp.126-134
[7] L. Tobarra, S. Ros, R. Hernández, R. Pastor, A.R. Gómez, A.C. Caminero, M. Castro, "Low-Cost Remote Laboratories for Renewable Energy in Distance Education", in Remote Engineering and Virtual Instrumentation (REV), 2014 11th International Conference, Porto, 26-28 Feb. 2014, pp. 106-111.
[8] Y. Karatepe, S.V. Neşe., A. Keçebaş, M.Yumurtacı, "The levels of awareness about the renewable energy sources of university students in Turkey", Renewable Energy, vol. 44, pp.174-179, 2012.
[9] P. Jennings, "New directions in renewable energy education", Renewable Energy, vol. 34, pp. 435–439, 2009.
[10] O. Benchikh, "Global renewable energy education and training programme (GREET Programme)" Desalination. Vol. 141, no. 2, pp 209–221, Dec. 2001.
[11] International Renewable Energy Agency, Second Ministerial Roundtable "The Role of Renewable Energy in Energy Security", Fifth session of the Assembly, Jan. 2015.
[12] S.C. Bhattacharya, "Renewable energy education at the university level", Renewable Energy, vol. 22, pp. 91–97, 2001.
[13] T. C. Kandpal, L. Broman, "Renewable energy education: A global status review", Renewable and Sustainable Energy Reviews, vol. 34, pp. 300–324, 2014.
[14] Republic of Turkey Ministry of Energy and Natural Resources Info Bank.[Online] Available:http://www.enerji.gov.tr/en-S/Pages/Electricity
[15] A. Karabulut, E. Gedik, A. Kecebas , M.A. Alkan, "An investigation on renewable energy education at the university level in Turkey", Renewable Energy, vol. 36, pp. 1293-1297, 2011.
[16] C. Acikgoz, A.A. Borazan, "Trends and Issues in Renewable Energy Education" in 1st International Conference on Foreign Language Teaching and Applied Linguistics (FLTAL'11), Sarajevo, 5-7 May 2011.

BIOGRAPHIES

VEDAT ESEN was born on June 30, 1982 in İstanbul, Turkey. He graduated from Marmara University, Technical Education Faculty, İstanbul, in 2009 and received M.Sc. degrees from Marmara University, Institute of Pure and Applied Sciences, in Istanbul, Turkey, in 2011. He has been started Ph.D. studying in department of Electrical and Electronics Engineering Marmara University, Institute of Pure and Applied Sciences in 2011. He is currently instructor in İstanbul Arel University. His current interests are power systems and renewable energy systems.

SEÇİL VARBAK NEŞE was born in Istanbul, Turkey. She received B.Sc. degree from Kocaeli University, M.Sc. degree from Afyon Kocatepe University and Ph.D. degree from Marmara University. She is currently working as a research assistant in electrical-electronics engineering department in technology faculty at Marmara University. Her interest areas are renewable energy systems, electrical power systems, signal processing and fault diagnosis techniques.

ŞAFAK SAĞLAM, was born on September 11, 1976 in Samsun, Turkey. He graduated from Marmara University, Technical Education Faculty, Istanbul, in 1997, and received MS and PhD degrees from Marmara University, Institute of Pure and Applied Sciences, in Istanbul, Turkey, in 2000 and 2006 respectively.

He has been employed as a research assistant and assistant professor in Technical Education Faculty between 1997 to 2012. Presently Dr. Sağlam is an Associate Professor in Technology Faculty Electrical and Electronics Engineering Department at Marmara University. His special fields of interest include renewable energy sources, illumination and power systems.

BÜLENT ORAL, was born on July 05, 1970 in Çorlu, Turkey. He graduated from Marmara University, Technical Education Faculty, Istanbul, in 1994, and received MS and PhD degrees from Marmara University, Institute of Pure and Applied Sciences, in Istanbul, Turkey, in 1997 and 2004 respectively. He has been employed as a research assistant, lecturer and assistant professor in Technical Education Faculty between1994 to 2012. Presently Dr. Oral is an Associate Professor in Technology Faculty Electrical and Electronics Engineering Department at Marmara University. His special fields of interest include energy policy, electricity market and renewable energy systems.

Balkan Journal of Electrical & Computer Engineering
BAJECE
An International Peer Reviewed, Indexed and Open Access Journal

ISSN: 2147- 284X
Vol: 5
No:1
Year: February 2017

CONTENTS

BALKAN JOURNAL OF ELECTRICAL & COMPUTER ENGINEERING

(An International Peer Reviewed, Indexed and Open Access Journal**)**

Contact
Istanbul Technical University
Department of Electrical Engineering,
Ayazaga Campus, Maslak, Istanbul-Turkey

Web: https://www.bajece.com
http://dergipark.ulakbim.gov.tr/bajece/
e-mail: editor@bajece.com